Gap Junction Ultrastructure Controversy Resolved in 3-D:

PITS AND PARTICLES DO NOT MATCH.

Introduction

This article aims at explaining why the widely accepted model of the ultrastructure of Gap Junction (GJ) should be revised. Current incorrect interpretation of the structure of this very important organelle of heart cells, which play a crucial role in the cardiac physiology, may prevent future progress in better understanding of the functions of cardiac and other tissues. Therefore, it is essential to have the model of the organization of this vital cellular detail updated.

P-face particles and E-face pits of freeze-fractured Gap Junctions (GJs) are widely considered to be complementary structures. In the present work, complementary replicas of GJs in freeze-fractured sheep cardiac Purkinje strands were studied using a new, original method for matching complementary features in the electron micrographs of complementary replicas by superimposing their stereo images. This method has never been used before. When a stereo image of a defined area of GJ E-face is superimposed on the stereo image of the corresponding area of P-face, the pits fall between the particles, not on them. Consequently, it is concluded that E-face pits and P-face particles are non-complementary.

For decades, a model of the GJ structure has been used in which the main component of GJ, the intramembrane particles (IMPs), are shown to be complementary with the pits. GJ particles are believed to shape the pits while being pulled out from the lipid bilayer in the processes of splitting the membrane to expose its interior. In the literature (and more recently on the internet) numerous diagrams are published of the GJ structure in which the complementarity of the GJ particles and pits is continuously suggested, as if it was a proven fact.

However, my observations (described in detail in this article) indicate that all these models may not be accurate in presenting the real relations between GJ components: particles and pits, seen in the cardiac cell membrane samples with EM. My critical review of the literature on the structure of GJs in the other types of cells indicates that the general model of GJ organization in other tissues (e.g. liver) of various species may also need to be revised.

Each GJ particle, or connexon, is believed to contain the channel which enables the intercellular communication. This channel is supposed to be continuous with its counterpart in the matching particle (connexon) located in the membrane of the next cell. The connexons are

believed to control the flow through the channels by opening and closing through structural changes of the protein molecules (connexin) which each GJ particle is built of.

In this widely used and accepted model the pits (found on the E-faces of freeze-fractured and replicated GJs) are assumed to be markers of the channels crossing the gap between the two membranes of the neighboring cells, which adhere tightly in the GJ region.

Such popular model, based on the widely spread and uncritically accepted principle of complementarity of particles and pits, has been consistently copied from one Cell Biology textbook to another (ref), and appears in every text related to GJ structure (ref). However, this popular model has never before been critically reviewed to determine if it really represents the true relations of pits and particles in the GJs.

In view of my findings, the idea of pits and particles being complementary (due to particles being pulled out of pits) may be purely speculative. Due to a lack of reliable published data, the attempts to correct the model were pretty rare (Kordylewski and Page, 1985a). Furthermore, some incomplete data available so far might have been used to support the traditional inappropriate model (De Maziere 1986), for lack of a better one.

My detailed observations of the fine structure of GJs indicate that pits seen in the split cell membranes can not be aligned with the tops of the P-face particles. I have observed that pits, which are a very distinct feature of the GJ E-face, do not lie on the same axis as the tops of the P-face particles. Through tedious analysis of multiple detailed electron micrographs of both faces in their complementary replicas, I demonstrated that the pits rather fall in the spaces located between the particles. Therefore, the pits cannot be part of channels contained in the connexons. Consequently, because pits are believed to be part of GJ channel, the focus of channel studies should also be directed to the space *outside* the connexons, rather than be confined solely to their interior.

GJ particles never occur nor function alone, but always form distinct aggregates in the plane of the membrane. There must be a reason why GJ channels are grouped so close to each other. This may additionally point to the importance of the interparticular spaces. If the connexons do not occur nor function separately, the spaces between neighboring particles must play role in holding them together to allow their synchronized action. Nevertheless, all studies of GJ channels are focused on the connexon and its interior. The idea that the channel might be located between the particles, where I find the pits, has never been considered. It might be also possible that nothing else but just the space between the particles could be where the channel is located. Such supposition is obviously contrary to the commonly accepted view that the channel is

contained within each particle (connexon). Nevertheless, the underestimated role of the spaces between the GJ particles must play some role in the coordination of the action of individual connexons. According to my studies explained below, pits seen on the GJ E-face are located right in this space.

Cell biologists often create impressive structural models which do not necessarily correspond well with the real cellular structures which they study with other then structural methods. In view of my findings obtained through detailed morphological study, such misinterpretation seems to happen in the case of GJ particles and pits. The limitations of the morphological methods, along with the recent decreased interest in traditional ultrastructural studies (TEM in particular) makes it difficult to verify models created by the researchers interested in other fields than description of the fine structure. Cell biology became dominated with computer generated, false color, processed images "confocal microscopy"-style, which are far from representing the real fine structure of studied cells. Molecular models are often designed using analogy with the macro world without having a critical look at the real details of the morphology of the presented microstructures, certainly not as they appear in original EM images. Single electron micrographs are frequently merely used to illustrate the studied structure, while drawing right conclusions requires analysis of great number of images.

Drawing a reasonable conclusion, in particular a conclusion that may aim at a major change of a popular, simple and impressive theoretical model (like that of GJ complementarity), requires tedious analyses of multiple images of fine structure. Such analysis requires working at the magnification levels next to the borderline of the available resolution, where an untrained eye usually sees very little. Meanwhile, attractive but not always true theoretical models are being developed that may fit available data, despite not being adequate to the actual structure. The true organization of the details may remain unclear because is not easy to interpret fine structure imaged on high power micrographs. In particular, recognition and elimination of the artefacts appearing in the sample due to the applied procedure is important to the right interpretation of the results and requires a lot of experience. Such artefacts may lead to errors in the correct understanding of the studied structure. Furthermore, it is even harder to show in a convincing way the controversial results to the others, who didn't have the chance to look into boring regularities in the multiple samples, did not do the tedious work themselves, may be biased by the "accepted models", and may not be ready to change their traditional textbook views.

Freeze fracturing of cardiac tissues

In the years 1982-1985, while being on the research team of Dr. Ernest Page at the Department of Medicine at the University of Chicago, I was carrying out studies of the quantitative evaluation of the

structure of cardiac cell membranes. At that time I mastered the preparation technique called freeze-fracturing (FF). Due to the quantitative character of my studies I had the opportunity of taking and analyzing thousands of high power photographs of the ultrastructure of cardiac cells and their membranes. This work resulted in a series of publications (Kordylewski et al., 1983, 1985a,b,c, 1986). In these papers the experimental methods used in this study are described in great detail.

Sample preparation

To avoid possible artifacts, tissues were obtained immediately after slaughtering the animals (sheep, rats, mice, frogs and chicks). In particular, sheep hearts were processed still at the slaughterhouse. Purkinje strands were quickly excised from the ventricular chambers and immediately immersed in 1.5% glutaraldehyde buffered to pH 7.4 with 150 mM Na cacodylate. The specimens remained in the fixative for one hour at 4° C while being transported to the laboratory. The Purkinje strands were then glycerinated and freeze-fractured with unidirectional shadowing on a Balzers BAF 301 apparatus (Fig. 1) and further processed as described by Kordylewski et al. (1983, 1985), except that the Balzers complementary replication device (Fig. 2) replaced the conventional specimen holder (Fig. 3). The same procedure was used for samples obtained from other species used in this study (rats, mice, frogs, and chicken).

Fig. 1. Balzers BAF 301 FF apparatus similar to the one used in this study. Vacuum chamber is seen in the centre where specimens were processed while being observed with binocular microscope. On the left are tanks containing LN2 hooked up to the apparatus. Sample stage was cooled with constant flow of LN2 when the specimens of tissue were fractured and shadowed with Pt/C.

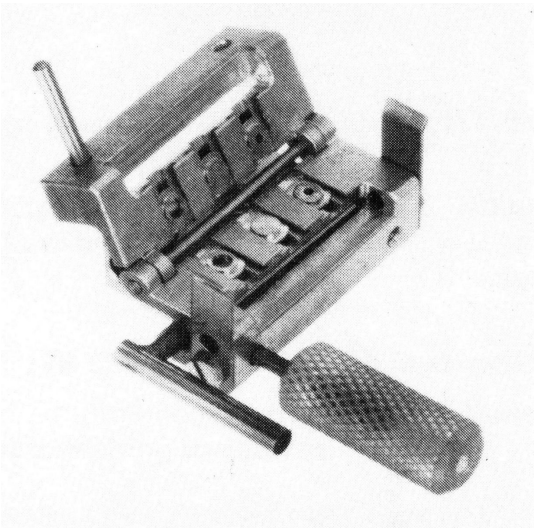

Fig. 2. BB 187 260-T Double replica specimen table for simultaneous production of three sets of complementary FF replicas. Three different samples of tissues were first sandwiched in the double holders, frozen with LN2 and placed in the slots of such table. No knife was used to expose the fractured surfaces. Instead, the upper half of the stage was rapidly lifted to open halves of the table like a book. At that time the tissue samples were being split into two complementary fragments which were immediately shadowed and replicated with Pt/C under high vacuum. In this manner each of the three samples yielded two complementary replicas which contained complete information of the fractured structures. The images of the complementary details, photographed at high magnification in 3D with the aid of EM could be then put back together by superimposing their images on films to see how they matched before fracturing and to demonstrate true complementarity of their fine structure (see Fig. 7).

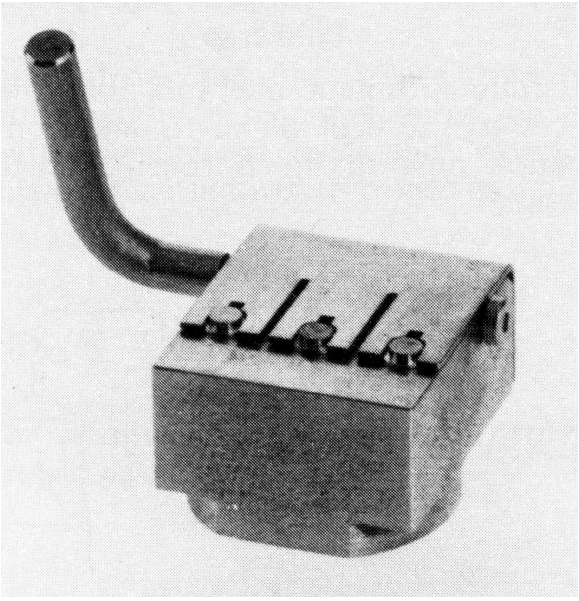

Fig. 3. BB 176 090-T Treble specimen table for simultaneous production of three non-complementary replicas of three different samples. Frozen tissue fragments were hold by a spring operated with a lever. After hitting the samples with a cold knife the exposed surfaces were immediately shadowed with the deposit of Pt/C under high vacuum. Such sample table is commonly used, although the upper portion of the frozen sample is removed with the knife and lost. Consequently the replicas produced with this table contain incomplete information about the sample. Only the surfaces in the saved lower part can be observed; their complementary details are not available.

The replicas were cleaned with Clorox and distilled water, collected on 300or 400 mesh uncoated finder grids and photographed at original magnifications of X 50,000 to X 200,000 in a Hitachi H-600 electron microscope (Fig. 4) equipped with a eucentric, side-entry goniometer stage and a Hitachi H 5001M multispecimen holder that permitted both alternate viewing of complementary replicas and tilting of the specimens. Stereo pairs were photographed at tilt angles of 5° with respect to each other.

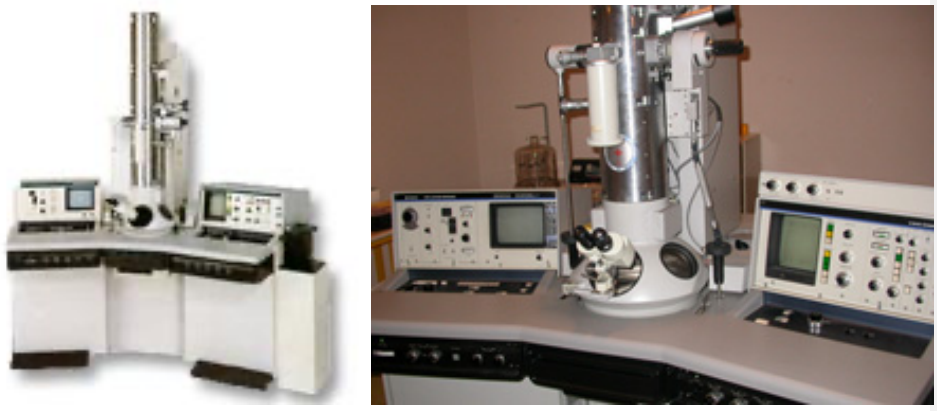

Fig. 4. Hitachi 600 transmission electron microscope similar to the one used in this study.

Techniques for comparing and superimposing complementary E- and P-faces of the same gap junction

Multiple techniques for investigating the complementarity of E-face pits and P-face particles in complementary double replicas of the same junction have been developed. The application of each technique was preceded by transilluminating on a light box the negative films of stereo pairs of electron micrographs of both complementary fracture faces photographed at original magnifications of X 50,000, X 100,000, or X 200,000, and inspecting them with a stereo viewer (magnification X 2), (Fig. 5) to yield a final magnification of X 100,000, X 200,000, or X 400,000.

Fig. 5. Stereo viewer.

In applying the additional techniques described below, such stereo views of the areas under study (like those in Figures 19, 21, 28, 29, 30, 42, 45, 46) were always at hand, so that the three-dimensional structure could be recognized and the landmarks of the gap junctional area could be identified. By consistent use of stereo views before applying other techniques, the areas least distorted by tilt or non-planarities of the surface could be selected. Furthermore, the preliminary stereo view was essential for aligning and then matching details of the E- and P-faces superimposed by various techniques with respect to external landmarks (most commonly either caveolar necks on the non-junctional plasma membrane cross-fracture edges or the boundaries of the gap junctional plaques). The structural features of the GJs (e.g., unusual arrays of particles, valleys between the particles, particle-free patches, etc.) have also been used as landmarks for matching the complementary details on the other face.

The additional techniques used included: (1) projection of complementary images on each other, (2) tracing projected enlarged images of pits and particles and comparing (superimposing) the tracings, (3) printing superimposed stereo images of complementary areas, (4) projecting superimposed stereo images on lenticular screen and viewing them with polarizing spectacles (like in 3D cinema), (5) mapping particles and pits and matching them by their individual numbers, (6) using a “blink microscope” (astronomical comparator) and (7) using a geological mirror stereoscope to identify matches. In the last two techniques the limitations of the instruments did not allow 3D images to be compared, therefore only single (non-stereo) images of complementary replicas were compared to find exact matches, although their corresponding 3D low-power views were always available for reference.

Technique 1.

Projection of a two-dimensional (non-stereo) image of the E-face onto a reverse-printed photograph of the corresponding area of the P-face (or vice versa) was performed with a darkroom enlarger. Both images, the one printed on paper and the complementary one projected from the original negative, were used at the same magnification. When a perfect match was found, the entire field was rather uniformly filled with matching complementary details. As long as the details were mismatched, high contrast discrepancies were distinct. It is important to note that the printed image had white shadows, while in the original negative projected on it the shadows remained dark. Despite this, finding the best match of corresponding particles and pits was usually quite easy.

Technique 2.

The negatives of an area containing P-face particles or E-face pits were projected onto the screen of a Nikon Profile Projector 6C-2 (Fig. 6).

Fig. 6. Nikon projection microscope 6C-2, similar to the one used in this study.

The negatives were enlarged 10- or 20-fold to give final

magnification X 10^6. The particle outlines were traced onto a sheet of tracing paper taped to the screen of the projection microscope. The negative of the P-face was then removed and replaced with the negative of the complementary area containing the E-face pits, aligned with respect to the landmarks as described above, and the locations of the projected pits to the outlines of the particles were determined. Also, both negatives were superimposed on each other on the stage of the Nikon Profile Projector and the alignment of the projected images was checked by flipping the upper negative and bringing it in and out of focus until the appropriate alignment was achieved. Then the edges of the negatives were secured by adhesive tape. In this way "double" negatives were made to print the middle composite picture in the triplets shown in Figures 20, 23, 31, 47 and 48). Also see Technique 3 below.

Technique 3.

An array of three contact prints from photographic negatives obtained on the electron microscope (magnifications X 50,000, X 100,000, or X 200,000) was mounted for each GJ photographed in 3D. The prints were aligned in such a way that each of the outer pictures in the set could be used for viewing as a stereo pair with the middle (composite) picture (Figures 20, 23, 31, 47, and 48). Figure 7 illustrates the four step sequence by which the final desired mounting was obtained.

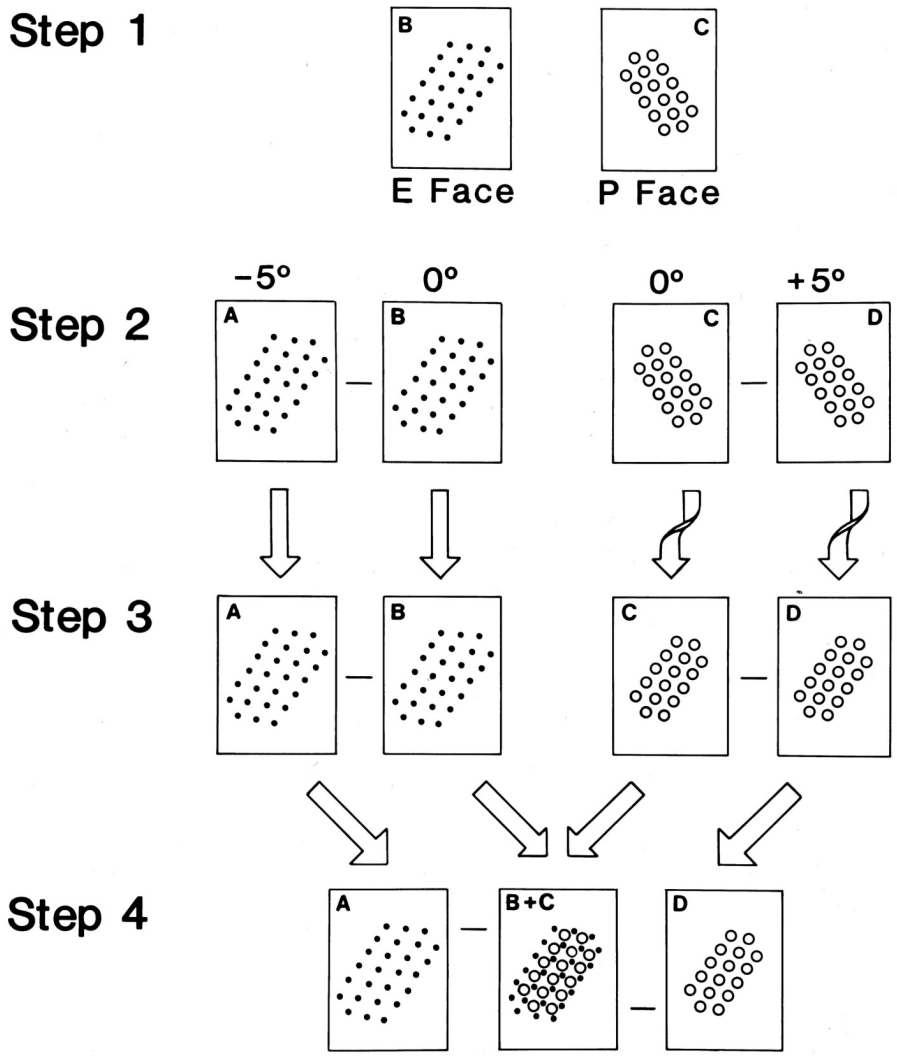

Fig. 7

The above diagram (Fig. 7) explains Technique #3 and illustrates the four-step sequence for aligning and mounting stereo images of complementary replicas to form an array of three photographs containing two stereo images as in the Figs. 20, 23, 31, 47 and 48).

Step 1 shows the complementary replicas of a junction photographed at 0^0 tilt; the pictures of two complementary replicas have been mounted in a conventional way, i.e., symmetrically, as they would appear if one opened the lipid bilayer like a book. Stereo viewing of both faces was more helpful for understanding the three-dimensional structure of FF GJs than conventional two-dimensional imaging. Therefore, stereo pictures of each complementary area (E-face and P-face) were routinely made by taking two pictures of the same area at a tilt of 5^0 with respect to each other (step 2). The stereo pairs of both complementary faces were then examined with a stereo viewer to check their planarity and to determine their three-dimensional features.

The superiority of stereo viewing over regular views of the replicas becomes apparent when the two types of images (planar and stereo) are compared, as in Figs. 18 and 19. However, a conventional comparison of pictures of complementary replicas mounted as "mirror images" did not allow sufficiently precise matching of complementary details (Fig. 19). In step 3 the negatives of the P-face stereo pair were therefore reversed by revolving them 180° around the long axis of the negative; as a result, the arrays of particles on the P-face stereo pair were parallel to the arrays of pits on the E-face stereo pair. Next, the two middle negatives (the members of each stereo pair photographed at 0° tilt) were superimposed (step 4). For this purpose the matching of landmarks and other details was checked by projecting the two superimposed negatives onto the screen of the Nikon Profile Projector 6C-2 (see above, technique 2). Then (as illustrated in Fig. 7), the resulting composite, or "sandwich", containing images of both complementary replicas photographed at 0° tilt, was mounted as the central picture of a three-print array; the left- and right-hand members of the array were, respectively, the -5° and +5° tilt members of the E-face and P-face stereo pairs. The two stereo pairs that can be looked at with a stereo viewer using this array are [A +(B + C) and (B + C) + D]. The center picture combines elements of both complementary E- and P-face images. Therefore, switching back and forth between binocular and monocular observations (by alternately obstructing one eye or the other) enables the viewer to obtain the projection of a non-stereo image of the particles onto a three-dimensional image of the corresponding pitted area (the left stereo pair); or the projection of the non-stereo image of the pits onto the three-dimensional image of the particulate area (the right stereo pair). The arrays of three prints in Figures 20, 23, 31, 47 and 48 should be viewed in this way with the aid of a stereo viewer. Exceptionally, all three prints of the set in Figure 33 were taken at 0° tilt since, when using the high magnification (X 400,000) needed for this array, a stereo effect could not be obtained. Nevertheless, even the naked eye inspection of the three picture arrays in Figures 20, 23, 31, 47 and 48 somewhat shows the relation between the complementary details.

Technique 4.

Superimposition of the stereo images of complementary replicas of gap junctional E- and P-faces using polarized light. For this purpose four Eastman Kodak slide projectors were equipped with polarizing filters. Two projectors were used to project aligned stereo pairs of a selected area of P-face onto a lenticular screen which was viewed through polarized glasses (Polarite 3D Viewer, Marks Polarized Corp., Whitestone, N.Y.). Two other projectors were used to project aligned stereo pairs of the E-face from the complementary replica on the same screen, so that (by the landmarks) the P- and E-faces were appropriately aligned. By rapidly alternating the projection between P-face and E-face, it was possible to achieve a "stroboscopic" effect that showed the location of complementary particles and pits relative to one another in three dimensions (3D).

Technique 5.

"Mapping" and numbering the GJs by inscribing the shapes of gap junctional P-face particles (as visualized in techniques 3 and 4, above) in the appropriate spaces between pits. The 3-M "Sensitron" Model 583 copier produced copies of the prints enlarged 20- to 50-fold. In addition to enlargement, the advantage of these copies was the high degree of contrast of all dark shapes, i.e., of the pits and the shadows of particles. By comparing these high-contrast pictures to the stereo images described in techniques 3 and 4, it was possible to identify each particle and to determine reliably its location on the fracture face as well as the location of the structure corresponding to it on the complementary fracture face. These particles were then numbered on the photocopied images of the P-face and the white areas corresponding to each number on the P-face were labeled with the same number on the complementary image of the E-face (Figure 34). After making "maps" of the complementary P- and E-faces and numbering them, the E-face map was overlaid with tracing paper and the pits identified on the map were traced and connected by lines with a sharp pencil (Figure 35 a and b); the particles on the map of the P-face were similarly traced (Figure 35 c). Next, the two tracings were combined (Figure 35 d) by superimposing them. The shapes of the spaces between pits were used to identify the corresponding particles (after first using tracings of structural features outside the junction for a preliminary orientation of the complementary replicas, as well as stereo viewing the superimposed images as in Figures 20, 23, 31, 47 and 48).

Technique 6.

Viewing two (non-stereo) images (negative films) of complementary

replicas with the comparator ("blink microscope"), Carl Zeiss Jena, Model 1638. This instrument, located at the University of Chicago Yerkes Observatory (Williams Bay, Wisconsin), was used by astronomers to compare photographs of the nocturnal sky taken at different times in search for new celestial bodies, like comets or new stars. A similar instrument was used to discover the planet Pluto (Fig. 8). Through quick alternate inspection of two similar film frames precisely aligned it allows to identify the same details in both pictures and helps finding possible differences. For my analyses similar instrument was also used later at the Cracow Observatory of the Jagiellonian University in Poland (Courtesy of the late Prof. Konrad Rudnicki).

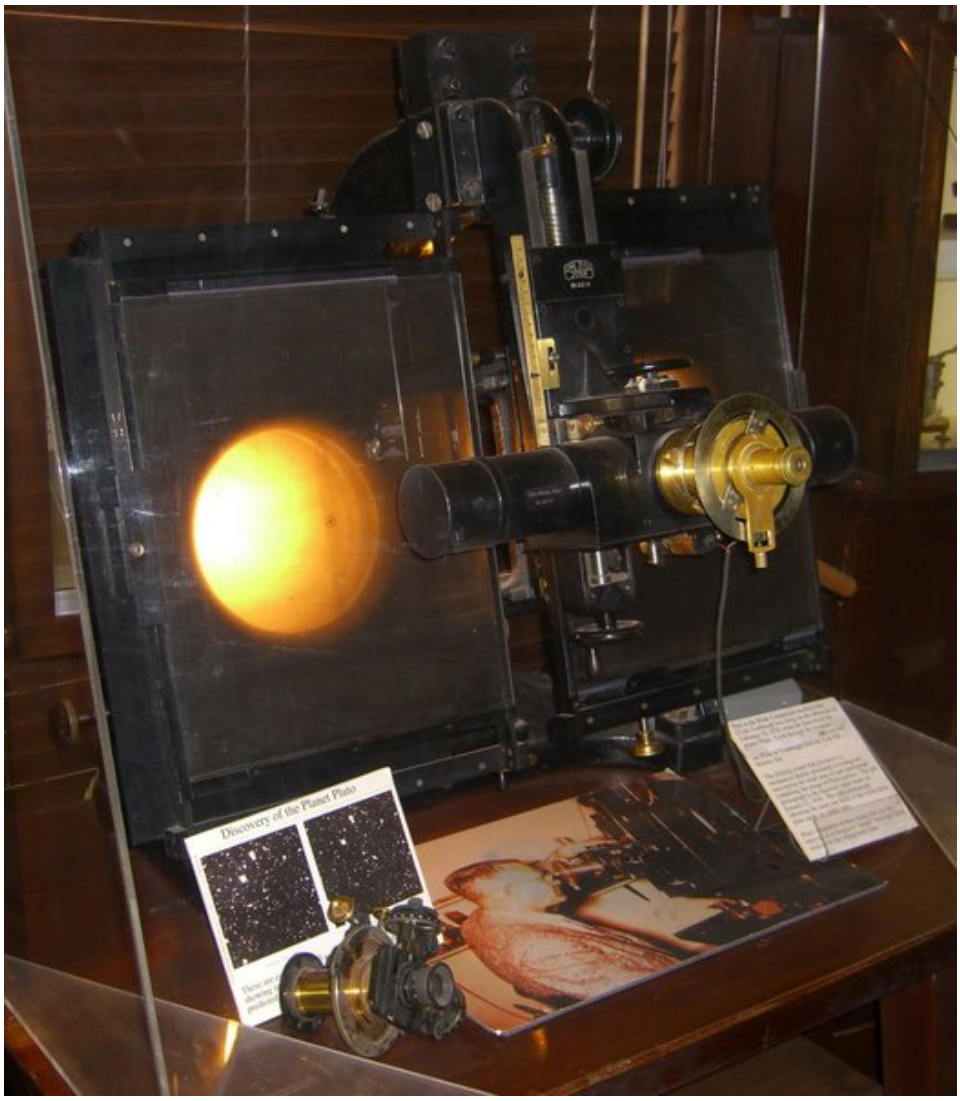

Fig. 8. Astronomical comparator (blink microscope), similar to the one used in the present study.

Although these instruments (blink comparators) produce planar rather than stereo images, their very high resolution is exceptionally good. They were originally designed to see small dots in the negatives marked by faint glow of remote stars. The images of GJ details thus obtained

could be related to that seen by stereo viewing, and could also be used to map particles and pits as in technique 5.

Technique 7.

Viewing prints of stereo pairs of complementary replicas with a large mirror stereoscope normally used for analysis of aerial photographs (Fig. 6). The instrument used was in the map collection of the University of Chicago Library. To use this technique, the prints of two stereo pairs were first precisely aligned and superimposed. By rapidly lifting the upper set of stereo-pairs and flipping between it and the underlying other set it was possible to alternate between stereo views of the P-face and the complementary E-face. In this way, thanks to the stroboscopic effect, the corresponding 3-dimensional structural features on the complementary replicas could be reliably identified and their locations on the complementary fracture faces could be compared.

Fig. 6. Mirror stereoscope used by geologists, designed for inspection of large format 3D aerial photography, similar to the one used in this study. Large working distance allowed rapid flipping between the two sets of printed stereo pairs, aligned precisely under the mirrors to see their best matching with the stroboscopic effect.

Unlike techniques 3 and 5, techniques 1, 2, 4, 6, and 7 do not yield publishable records.

Interpretation of the images of the freeze fractured membranes

The freeze fracturing procedure is believed to split the membrane open along the space contained in the lipid bilayer, between the lipid layers (see color diagram below in Fig. 7).

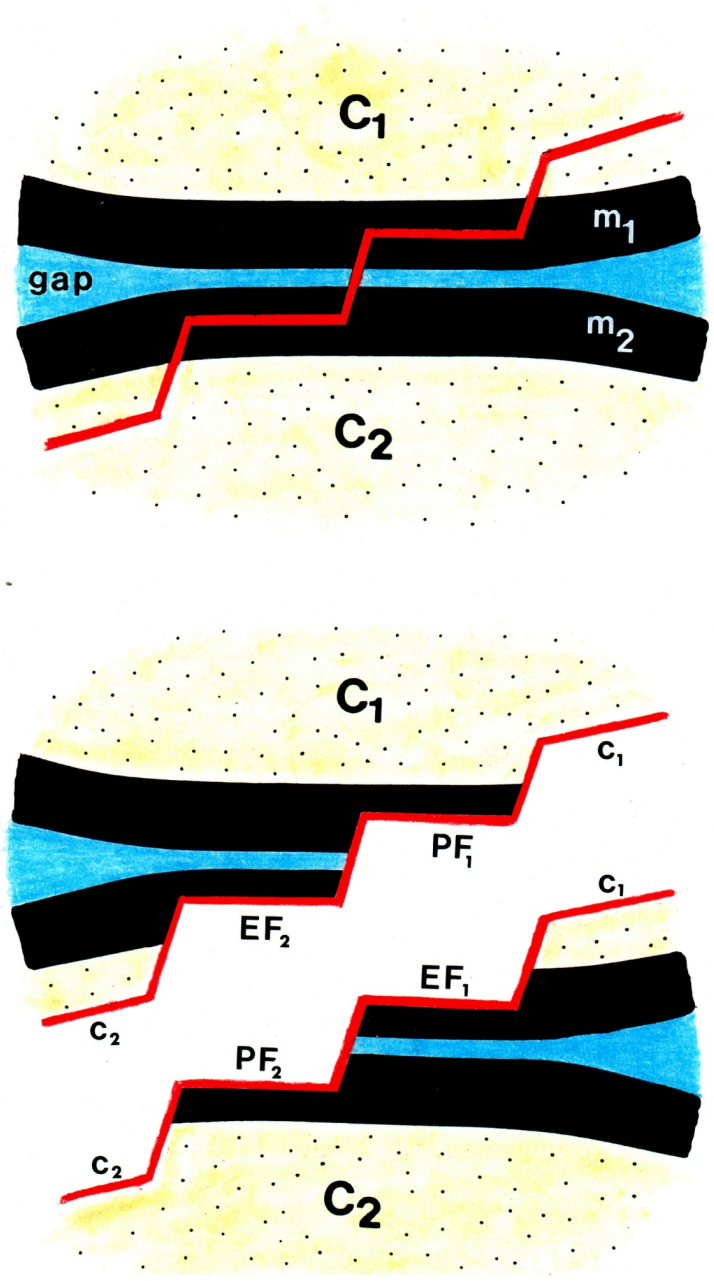

Fig. 7

In this "hamburger" diagram (Fig. 7), fragments of two cells (labeled C_1 and C_2) are shown in the area of GJ joining these two cells. The diagram illustrates the relations of the cells, as if they were seen in a traditional ultrathin cross-section, not in a freeze-fracture replica. The fracture planes (red) are mostly oriented perpendicularly to the plane of this cross-section.

In the above diagram (Fig. 7) the intercellular space is marked blue. It narrows in the GJ region where the membranes of two cells adhere closely and limit the space between them to a narrow gap. This diagram helps to understand the various areas in the replicas viewed with EM. The relation of this diagram to the actual images of the (complementary) replicas is explained in Figs. 15 and 16.

Here in Fig. 7 the replicated surfaces exposed with freeze fracturing are marked red. The other "split mattress" diagram, which correlates the cross-section of the GJ with the topography of GJ split by freeze fracturing, is shown and explained further down the text in Figs. 15 and 16. This diagram in Fig. 7 will be later compared also with the more detailed diagram in Fig. 17.

In Fig. 7 the upper part of the diagram shows the situation exactly at the moment when the knife hits the yet intact sample, causing the crack travel through the frozen sample along the plane marked here as red zigzag line. The cytoplasms of the neighboring cells (C_1 and C_2) are shown as dotted yellow fields. For simplicity, the cell membranes (adhering closely in the GJ area) are presented as single parallel black zones (m_1 and m_2), while the structural details of their lipid bilayers and particles (connexons) are not shown at all in this figure. The crack (red), which is believed to open the membranes in the process of freeze fracturing in the middle between their bilayers, starts in the body of the upper cell C_1 and travels down (from right to left) from the plane of one membrane (m_1), across the narrow intercellular space (blue), into the plane of the other membrane (m_2). Note that the intercellular space (blue) is narrowed to a "gap" in the region of the junction of the two cells. The crack eventually leaves the membrane plane and goes down to the left into the cytoplasm of the lower cell (C_2), similarly as it started in the cytoplasm of the upper cell (C_1) on the right.

The lower part of the diagram (which shows the other "hamburger" already split into two halves) illustrates the situation *after* the membranes are crack open. The upper part of the specimen (containing mostly cell C_1) is usually removed and lost. Only the surfaces on the lower part of the sample are exposed and made available for replication through shadowing with platinum and carbon (Pt/C).

At this point it is important to clarify that the person performing freeze fracture cannot control how the crack travels across the frozen tissue. The crack passes through the specimen hitting various cell

components at random. The abundance of various broken surfaces is exposed and replicated; they are later identified visually in the TEM and selected in search for the useful areas of exposed membranes, which are finally photographed at high resolution.

In Fig. 7 the crack (red) is shown to expose parts of the cytoplasm of cell number 2 (C_2), but some fragments of the body of cell number 1 (C_1) may also be seen in the split sample. Again, going from right to left, the exposed surface of the sample, subsequently shadowed with platinum and carbon (red), contains areas of the cross fractured cytoplasm of the upper cell (c_1) next to the areas showing the interior of its membrane (EF1). The crack never follows the outer surfaces of the membranes, thus the interior of the gap in GJ (marked blue) is never exposed. After the crack passes across the gap into the membrane (m_2) of the other cell (C_2), it continues along the interior of that membrane (PF2). Eventually it exposes also the interior of cell C_2 (left).

The cytoplasm cross-fractures, seen as rough areas in the replicas, do not contain any relevant information and are usually avoided when electron micrographs of the replicas are taken. On the contrary, the replicated surfaces of the interior of the membranes show quite spectacular details, after the replicas are later seen with EM, particularly in 3D.

The upper portion of the lower diagram is usually removed and lost in the routine freeze fracture procedure. However in my studies it became crucial to save the upper portion of the same sample and produce the second, complementary replica. Use of the double replica table (Fig. 2) made it possible. Both replicas obtained from the two parts of the split sample were complementary to each other and their structural details and relations will be described and discussed later.

Particles distinctly seen in the replicas of the freeze fractured membranes were in the main focus of my studies. These particles are supposed to consist of protein aggregates, which (after opening the frozen membrane) are observed spread over the exposed smooth inner surfaces of the split lipid bilayer (see four electron micrographs below). For the reason unexplained so far, the frozen membrane tends to split asymmetrically, leaving more numerous particles on one side (called P-face), while the other side (called E-face) is less densely populated with protein particles. In the GJ area, E-face does not show the presence of any particles, which occur only on the P-face, and are usually larger that the non junctional particles. Particle-free E-face of GJ membrane is populated with numerous smaller pits. According to the traditional understanding of how GJ splits, pits are believed to be complementary with the particles. In the “hamburger” diagram above, these different faces of the split membranes are labeled EF1 (E face of the membrane of cell 1) and EF2 (E face of the membrane of cell 2), PF1 and PF2, respectively for P-faces of both these cells. The detailed relations of pits and particles are not shown in this diagram in Fig. 7.

They are discussed in detail in the description of the "split mattress" diagram (Figs. 15,16, and 17).

Non-junctional membranes

While performing my quantitative studies I became very skillful in recognizing the ultrastructural details of cardiac cells and their membranes. I went through thousands of images that seemingly looked the same. I knew the split cardiac cell membrane structures by heart and I was able to identify them easily. These skills allowed me to later identify and correlate the corresponding structural details in the same freeze-fracture replicas with TEM and ATM. The subsequent publication (Kordylewski 1994) represents one of the first pioneering works in the area of Comparative Microscopy.

My published comparative and developmental studies on the images of cardiac membranes of various species (rat, sheep, chicken, and frog) demonstrated species-specific quantitative differences in the numbers and sizes of the particles (Kordylewski et al., 1983, 1985b, 1985c, 1986). The examples of such differences are given below in Figs. 8 – 11, which show vast nice areas of P-faces of non-junctional membranes.

The images of the non-specialized regions of the membranes, which occupy most of the cell membrane, are generally uniform in appearance. The external leaflet of the membrane does not show the presence of pits and is less populated with particles than the inner leaflet of the cell membrane, P-face. P-face is characterized by greater density of the particles, randomly spread over the inner surface of the membrane, after being exposed by FF. Particles, which are assumed to be the protein component of the membrane, for some unknown reason seem to adhere stronger to the inner leaflet of the membrane than to the outer layer. It is also possible that their uneven partition between the split leaflets of half-membranes results from their original asymmetric allocation in the native unsplit membrane. It is also possible that the membrane splits asymmetrically in the FF process. Nevertheless, the exposed surfaces are believed to be always the inner surfaces. Neither the cytoplasmic surface of the cell membrane nor the outer surface of the cell membrane are ever exposed by FF. This technique seems to open membranes along the space between the lipid monolayers, the particles (protein aggregates) being pulled out of the sandwich of the bilayer. The exposed surface of the monolayers shows in the electron micrographs as a smooth background for the particles spread over it at random.

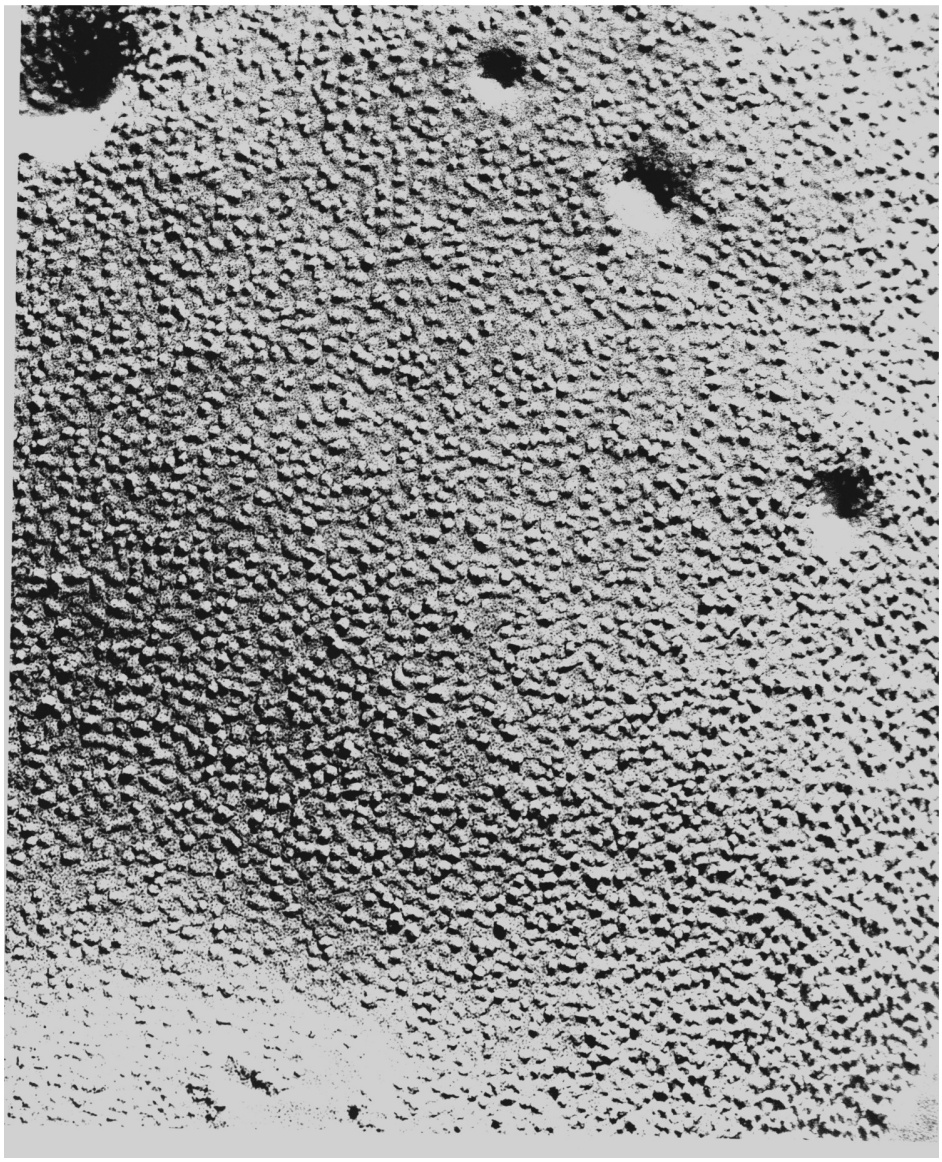

Fig. 8

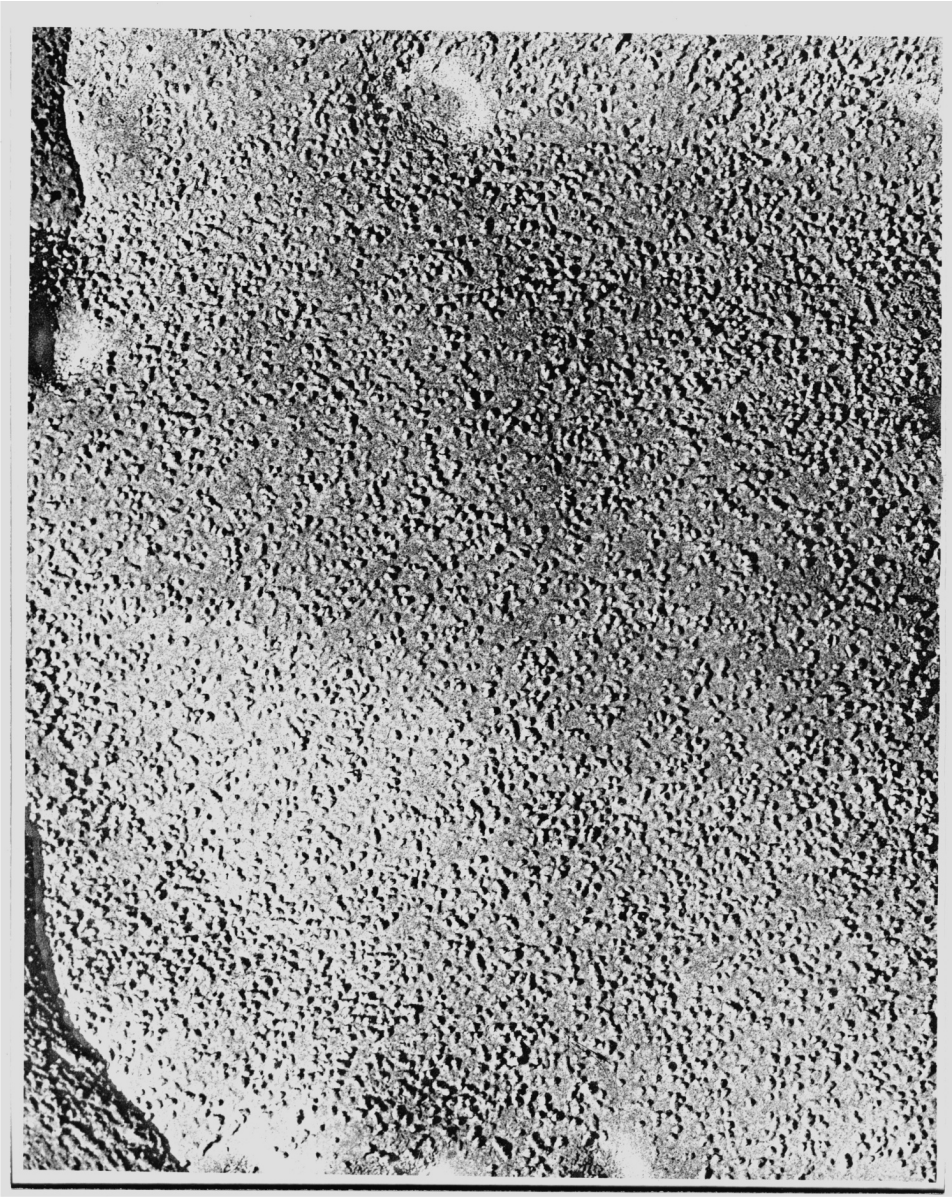

Fig.9

Fig.10

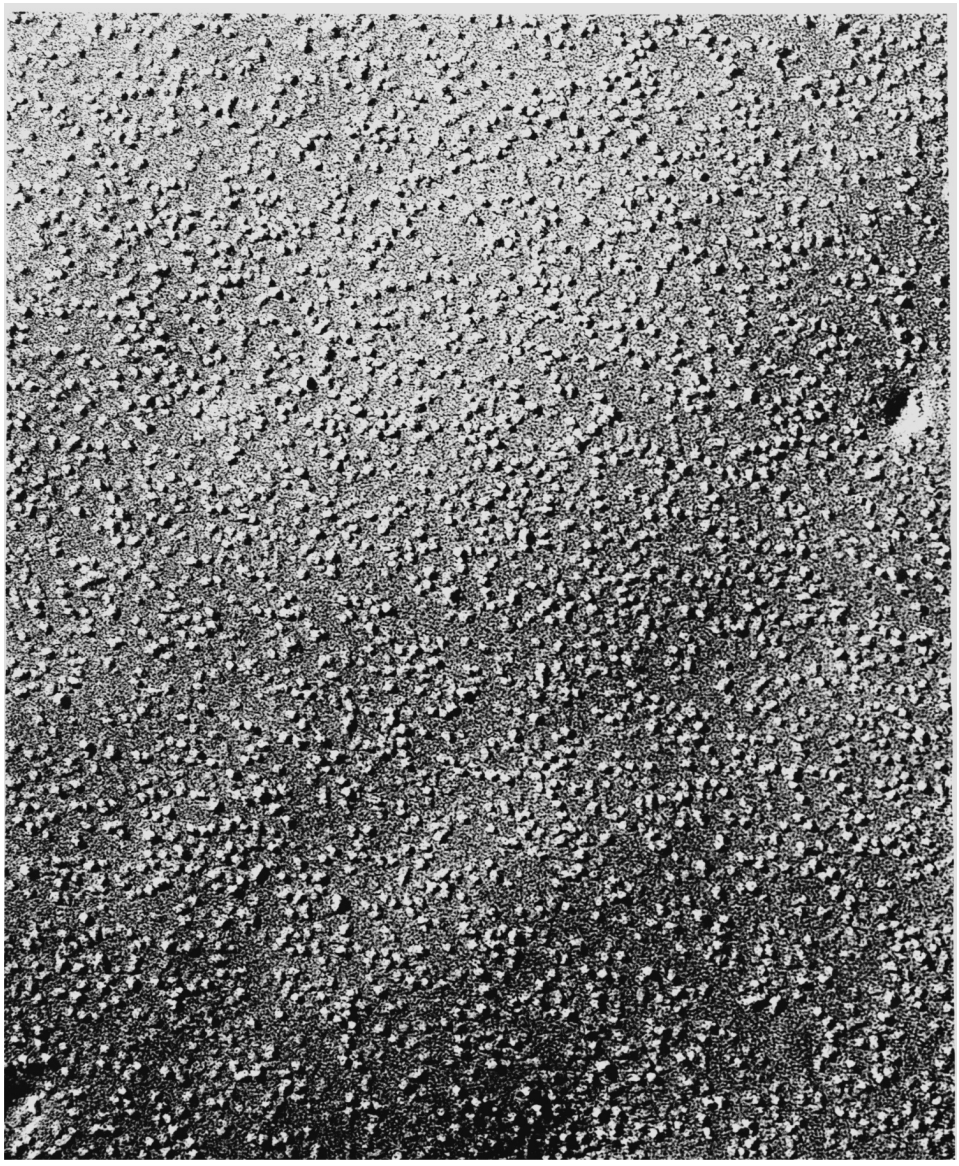

Fig. 11

Besides numerous particles, larger depressions in the surface are seen in these micrographs of the freeze-fractured membranes (Figs. 8-11), which are called “caveolae”. Some of the fully developed caveolae

apparently broke off at their neck level, giving appearance of a smaller hole in the continuous membrane, filled with the contents of the caveola (Fig. 11 and arrow in Fig. 28). The quantification of the caveolae was the subject of my separate study (Kordylewski et al. 1993).

Junctional membranes

While looking at the freeze-fractured membranes and selecting suitable areas for taking hundreds of EM micrographs for my quantitative analyses of particle distribution, I repeatedly went across specialized areas of the cell membranes, which contained cell junctions. In particular, Gap Junctions (GJs) were attracting my attention, due to very characteristic patterns of the array of their particles. The junctional particles are usually larger in size than the particles outside the area of the junction.

Electron micrographs of freeze-fractured tissues containing GJs show characteristic patterns of more or less regularly arranged particles and pits on the P- and E-faces of the fractured membrane (Peracchia, 1980. Current concepts of GJ structure regard the particles and pits as complementary structures which result from the splitting of the connexon, an assembly of integral membrane proteins made up of six identical polypeptide subunits surrounding a central channel (Makowski et al., 1977, 1984). The interpretation of P-face particles and E-face pits as complementary implies that in the native (*in situ*) state, the structures from which these two components originated lay on the same transmembrane axis, and that the transmembrane axes of the particles and pits are identical and correspond to the locations of the cell-to-cell channel. It is widely recognized that the E-face pits of GJ are more closely spaced and more highly ordered than the P-face particles (Peracchia, 1980). These discrepancies are reconciled with the supposed complementarity of particles and pits by postulating that distortion of the native connexon array by "plastic deformation" during freeze-fracture affects the P-face particles more than their complementary E-face pits (Peracchia, 1980). Complementary replicas of GJ investigated recently in freeze-fractured Purkinje strands from sheep hearts exhibit structural characteristics inconsistent with the notion that their particles and pits are complementary. In the present paper a new method of matching complementary features is described. It involves superimposing stereo images of the complementary replicas. When the stereo image of a defined area of E-face is superimposed on the stereo image of the corresponding area of P-face, the pits fall between the particles, not on them.

Frog Gap Junctions

GJs seen in the frog mostly show a pattern of assemblies of circularly arrayed particles, as illustrated in the electron micrograph below (Fig. 12):

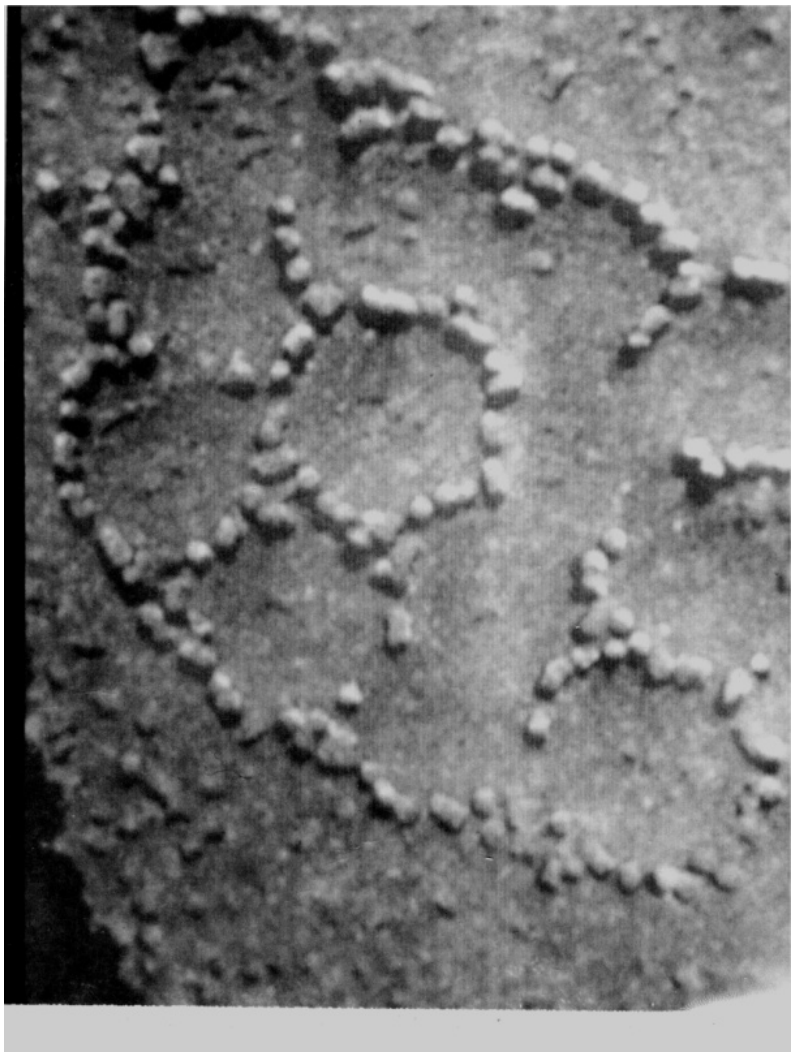

Fig. 12

Mammalian GJs are known to have particles assembled more tightly, “squeezed” into characteristic hexagonal arrays, which is distinctly seen in the majority of electron micrographs shown below.

Most of the observed gap junctional particles displayed regular globular shapes, while some were larger or irregular, possibly due to fusion with a neighboring particle. Additionally, some hypothetical “preparation artifact” (plastic deformation) could be the factor affecting the appearance and distribution of the particles due to freezing and fracturing of the sample. Although the shadows of the particles (created by oblique deposits of platinum and carbon of which the replica of the frozen and split cell membrane was composed) were usually enhancing the image of most of the particles, some particles could have been ill defined while obstructed by a shadow of a neighboring particle. However, through using high power magnification 3-D images (up to 500,000x), I was able to trace and count each and all particles in the junction (as seen in the example of a circular frog GJ below),

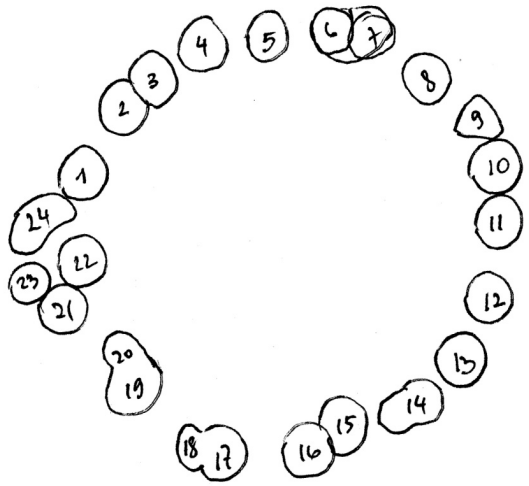

Fig. 13

as well as examine their distribution with remarkable accuracy.

Stereo imaging

For better recognition of particles (as distinct bumps elevated over the smooth half of the lipid bilayer), I routinely took two pictures of the same area. While taking pictures with the EM (Hitachi 8000)equipped with the goniometer stage, I always tilted the specimen by at least 5 degrees between the subsequent shots. In this way I produced stereo-pairs of the images of the viewed area. Each of the two pictures contained the same structures photographed at a different angle. Such paired photographic images (Figs. 19, 21, 28, 29, 30, 42, 45 and 46) were recorded on a film as original negatives. The paired negatives were examined on a light box with stereo viewing glasses. The pairs were precisely aligned to create a 3D effect. Their prints on paper were mounted in a similar way. To obtain the 3D effect they should be inspected with stereo glasses, or the X-3D viewing with the naked eyes should be used.

The same 3D imaging method was also helpful in identifying the non-junctional particles, for my quantitative analysis of the membranes (Kordylewski et al., 1983, 1985b, 1985c, 1986). Once identified three-dimensionally, the particles could be more easily traced and counted.

True gap junctional structure

The asymmetric splitting of the lipid bilayer in the GJ regions results in a different appearance of the junctional membrane on the P- and E- faces. While P-face shows GJ particles nicely arrayed, E-face of the GJ is totally free of the particles. Instead of particles, the lipid bilayer surface shows the presence of distinct, darkly shadowed pits on the E-face. The arrays of pits and particles are more or less regular, forming circles in the case of frog GJ or showing approximately hexagonal pattern in the other examined species.

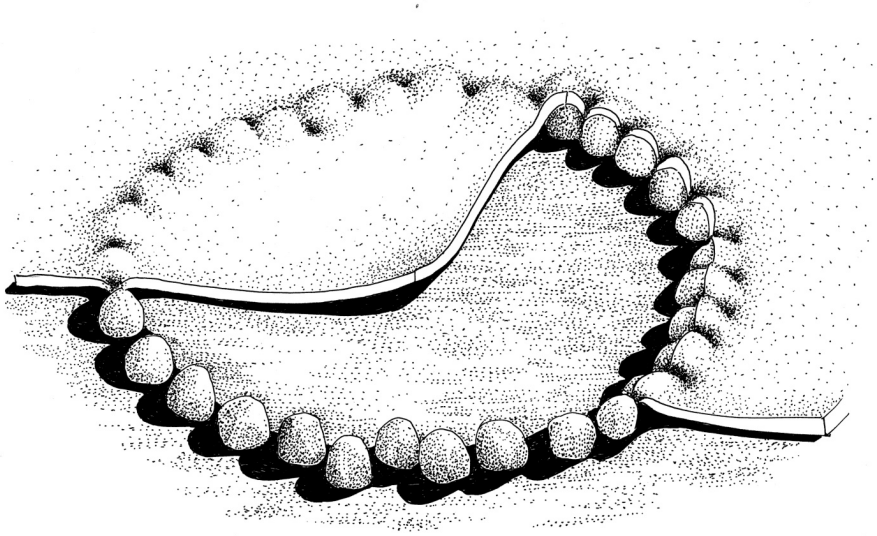

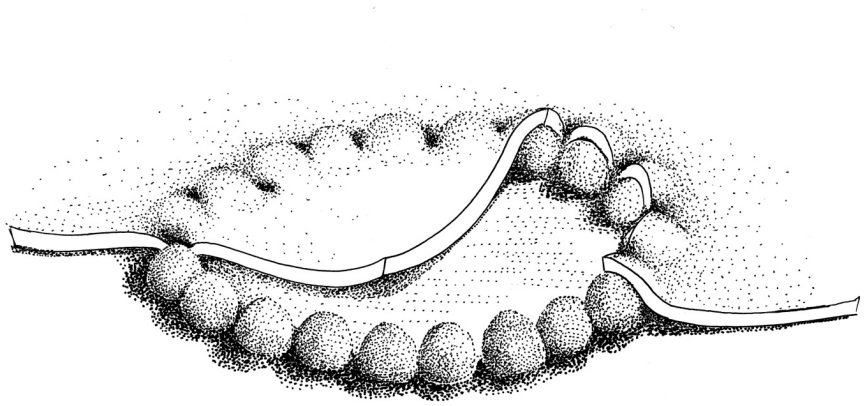

Fig. 14

The above “apple pie” diagrams show the artist’s rendition of a frog heart GJ based on my observations. GJ particles are arrayed in a circle on a smooth half of the lipid bilayer, whose interior is exposed due to freeze-fracturing. Most of the GJ area shown in Fig. 14 is composed of the P-face of the gap junctional membrane (m2 in Fig. 7) of the cell whose cytoplasm lies underneath (C_2 in Fig. 7). The P-face, populated by the GJ particles, is partially covered by the layer that belonged to the membrane of the upper cell (C_1). This upper cell was removed by freeze-fracturing, however,the patch partially overlaying the P-face particles represents the external half of the lipid bilayer of the upper cell (C_1) and is called the E-face of the GJ membrane. The actual “gap” of the GJ is contained within this layer, because the FF crack never separates the membranes along their external surfaces, but rather travels from within the plane of one membrane, (splitting their lipid bilayers and exposing the membrane interior), to the plane of the other membrane, crossing the extracellular gap. The appearance of the pits has been drawn in this diagram as closely as possible to their real appearance in the GJ E-face seen in the electron micrographs. The pits are obviously not the depressions that would be imprinted by the removed set of particles of the upper cell. They clearly show as distinct darkly shadowed depressions between the particles of the lower cell, as if the overlaying E-face of the upper cell membrane was molded around them in the GJ region. Similar relations of the GJ pits and particles are illustrated in the “open mattress” below, which relates to the mammalian GJ.

The corollary of the complementarity of particles and pits has been

coined by earlier investigators, who routinely examined only the neighboring P-face and E-face surfaces in single images of GJs. They never looked into 3D images of complementary replicas, which I decided to consistently use while examining the ultrastructure of freeze-fractured membranes and GJs.

Therefore, for these authors merely considering similar array of pits and particles in the neighboring (non-complementary) areas, it was natural to believe that the pits observed on E-face may represent "scars" after the corresponding particles have been pulled out of the lipid bilayer. Consequently, it has been concluded that those openings may mark the presence of the GJ channels in those locations. However, such hypothetical conclusions were drawn based on the examination of the analogy of the pattern observed on the neighboring areas of P- and E-faces, never through examination of the complementary areas of the same region of both halves of the same GJ. In my studies I always compared the corresponding E- and P-faces of exactly the same areas in complementary replicas of both halves of the same split GJ. Therefore my conclusions, resulting from more detailed, exact examination, did not agree with the widely accepted, but not verfied model. Unfortunately, these incorrect models found their way to all Cell Biology textbooks and basic text on GJs , and are continuously cited and uncritically repeated.

In traditional freeze-fracture studies, the frozen sample is hit by the knife and the sample cracks along the cell membranes, splitting their bilayers. The lower portion of the sample is then shadowed with platinum and carbon, while the upper part, containing the complementary sections of the membranes and junctions, is usually lost. Therefore the conclusions regarding matching and complementarity have been drawn from looking only at the neighboring analogous regions, because the complementary areas are not available. In my studies, thanks to using a specially designed complementary stage of the freeze-fracturing apparatus, I was able to save both halves of the split specimen and consequently replicate them both at the same time. Matching the high power images of the complementary replicas and finding the complementary details that originally formed one piece before fracturing was not an easy task. While doing this research I applied techniques similar to the methods used by contemporary forensic trace analysts, who routinely perform examinations of matching fracture surfaces of macroscopic objects found at different locations, to determine if at one time they could have formed a single object (Saferstein, 2002). Similarly, dactyloscopy compares fingerprints with actual ridged patterns of the finger tips. Although none of them are identical, they have to display similarity beyond "reasonable doubt" and match in order to lead to positive identification of a person.

In this way the traditional, widely accepted (but not verified) belief that pits and particles are complementary structures has been effectively challenged by the results of my observations carried on 3D

images of complementary replicas of the same GJs.

I published my conclusions in the form of an abstract (Kordylewski and Page 1985a), which preceded the presentation of my results at the Meeting of Biophysical Society in Baltimore in spring 1985. Much to my disappointment, although at the Meeting I have shown my images of both faces in 3D on large lenticular screen to the audience wearing 3D polarizer spectacles (see the description of Technique X), my challenging the popular and widely accepted concept that E-face pits and P-face particles are complementary was met with skepticism and disbelief. Therefore, my results, prepared for a full-length paper, have never been published. Despite the biased criticism I still believe that my observations give a better, more adequate explanation of the fine structure of GJs.

New GJ model

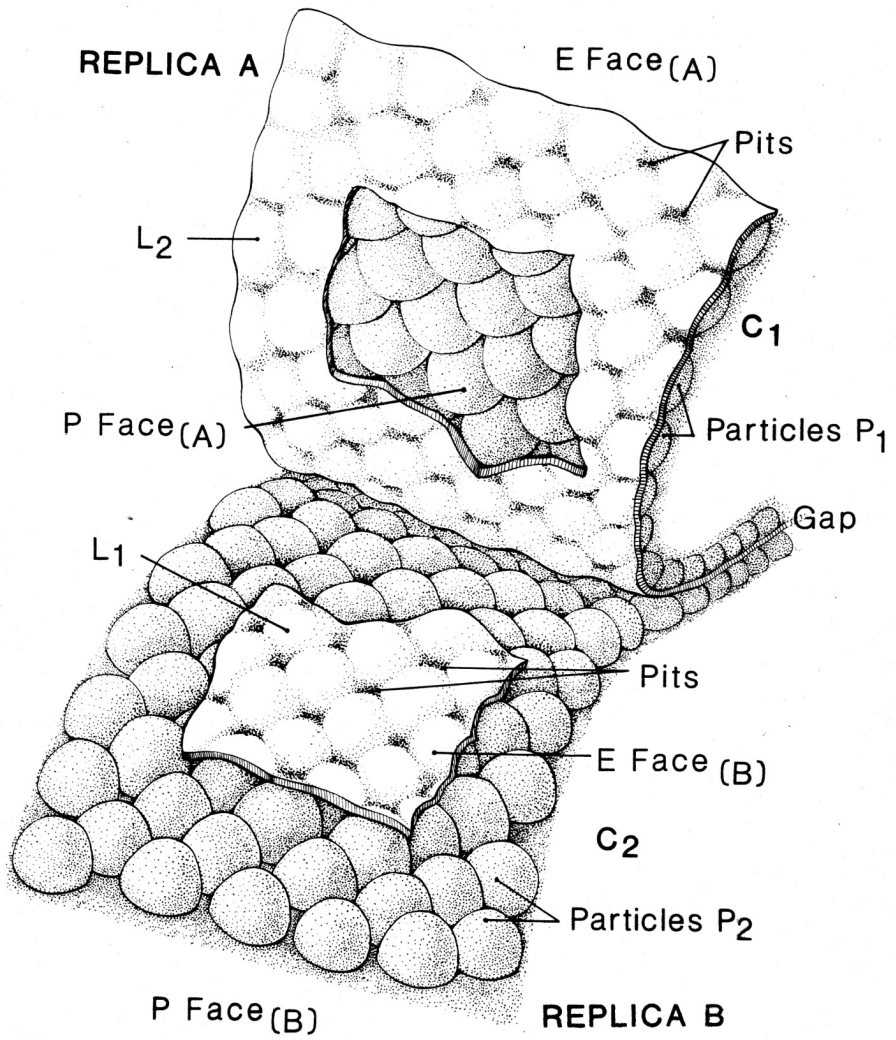

Fig. 15

The "split mattress" diagram above contains an artist's drawing depicting a model of a GJ based on my conclusions regarding the lack of complementarity of GJ pits and particles. It shows the GJ that has been

split into two complementary replicas (A and B) in the process of freeze-fracturing the two cells (C_1 and C_2). Before splitting, the plasma membranes (m_1 and m_2) of these cells (C_1 and C_2) came together to form the junction. The cytoplasm of cell C_1 may be imagined to lie behind the upper part of the split junction (A); the cytoplasm of cell C_2 lies below the lower part of the junction (B). The lower part of the model shows predominantly the particulate P-face of the membrane of cell C_1, the upper part the corresponding pitted E-face of the same membrane split open. For simplicity, the central depressions (which are rarely seen on tops of the replicated particles, but are thought to be the central channels) are not indicated. The intercellular gap is shown in a cross-fracture of the junction on the right. The side view in this region of the diagram refers to the traditional images of GJs in the TEM images of ultrathin sections of GJs. Since the fracture plane was never seen to follow the gap, the gap is not shown where the junction is fractured en face. The gap is probably contained within the layer L, while the fracture plane steps from one side of the layer (L_1) to the other side (L_2). This has been discussed above when the trail of the fracture in the "hamburger" diagram was described (Fig. 7).

The presence of a common layer (L) separating the two sets of particles (P_1 and P_2) from the two cells (C_1 and C_2) becomes evident by three-dimensional visualization of the complementary replicas using stereo imaging as in most double or quadruple panel figures below. The E-face always appears pitted after unidirectional shadowing, whether (as L_1) it belongs to cell 1 or it belongs to cell 2 (as L_2). The diagram illustrates a patch of the pitted layer L_1 which has become detached while being fractured from the upper half (A). The patch remains with the particulate surface (P_2), thereby leaving the central opening (window) in the pitted area of the upper half (A). Through this window a set of particles (P_1 of cell C_1) can be seen by examining the E-face of replica A. The detached patch overlies the particles (P_2 of cell C_2) that show up as the particulate P-face on replica B. The particles P_1 originate in the membrane of cell C_1, and the particles P_2 originate in the membrane of cell C_2; i.e., during freeze-fracture, the membranes separate so that P_i travels with C_1 and P_2 travels with C_2. By contrast, during freeze-fracture the membranes separate so that the E-faces are exchanged between the cells: Viewed from above, the patch of pitted E-face labeled L_1 (which forms the top of a composite layer into which the particle of replica B can be seen to bulge) originated from the membrane of the upper cell (C_1). The pitted surface L_i is the external leaflet (E-face) of the membrane of cell C_1. The area (L_2), which remains with the upper cell (C_1) after the "window" (L_1) has been removed, originates from the E-face of the membrane of the lower cell, C_2.

A new model of Gap Junctions.

It is convenient to describe the results of experiments on the spatial relationships of gap junctional particles and pits with

reference to the model or "cartoon" in Figures 15 and 16.

The model was drawn by an artist on the basis of data obtained using the methods described in the Methods section and in the paragraphs to follow. Reference to this drawing in Figures 15 and 16 will facilitate discussion of the structural features in the electron micrographs of complementary replicas (Figures 18-33 and 44-48). The drawing in Figs. 15 and 16 depicts a GJ that has been split into the two complementary replicas A and B in the process of freeze-fracturing the two cells, C_1 and C_2, which are coupled by the junction. It indicates how the component membranes of the GJ fracture in the observed complementary replicas. The diagram illustrates that the E-face appearing in complementary replicas is always derived from the membrane of the same cell as that from which the complementary P-face originates. As noted by Peracchia (1980), the *en face* fractures through the plane of the intercellular gap do not occur; hence the gap was not visualized in the complementary replicas. A noteworthy feature of this diagram is that in unidirectionally shadowed complementary replicas the E-face pits appear as depressions no matter from which of the two cells making up the junction the E-face is derived. A second noteworthy feature illustrated in the model, one which can readily be confirmed by stereo viewing appropriately mounted electron micrographs as in Figures 19, 21, 28, 29, 30, 42, 45 and 46, is that the E-face areas between the pits appear convex because they are bulged upward by the P-face particles that lie directly under these areas, covered by the "lemon frosting" E-face layer (layer L1 and L2) in which pits are present (Fig. 18). Figures 18, 22, 24 and 44 show the complementary fracture faces of GJs mounted in the "open book" configuration for non-stereo viewing, as shown in the drawings in Figs. 15 and 16 and explained in step 1 of Figure 7. This and all other electron micrographs were double printed so that particles appear white, whereas pits and shadows of the particles appear black.

In Figs. 18 the symmetry of the complementary junctional fracture faces is apparent, as is that of the caveolar necks whose complementarity is evident near the top of the picture. In Figure 19, the two complementary replicas of Figure 18 were photographed as stereo pairs of each replica and mounted for separate stereo viewing of each replica (as in step 2 of Figure 7). This way of mounting and viewing facilitates recognition of the layered structure of the junction and of the way the junction splits into the complementary replicas. In Figure 20, the stereo pairs of the complementary replicas of Figure 19 have been mounted as described in Figure 7 (step 4). This way of displaying, as well as similar but somewhat more favorable 3-fold arrays in Figures 20, 23, 31, 47 and 48, demonstrates that the pits on the E-face overlie the spaces between particles on the complementary P-face. Conversely, the pattern of P-face particles can also be traced on the E-face. In the composite central panel (Figure 20) the branched pattern of the E-face seen in the left panel is exactly filled with the particles lying in the same area of the P-face in the right panel. Figures 21 and 23, photographed at a higher magnification of X 10^5, reinforce these

conclusions. The branched pattern in Fig. 20 corresponds to the “window” in the “split mattress” model in Figs. 15 and 16.

Figures 24-32 and 44-48 show complementary replicas of GJs which chanced to fracture in such a way that only the pitted E-face appeared on one replica and only the particulate P-face appeared on the other replica. Therefore, unlike the complementary replicas of Figures 18-23, no patches of E-face (or “windows”) are shared by both replicas in these images (Figs. 24-32 and 44-48). It is nevertheless clear from Fig. 25 (and 27) that a layer of particles is present under the E-face of the lower stereo pair; the evidence is the bulges of the area between the pits by which the underlying particles manifest their presence. Stereo viewing of Figures 28-32 and 10 supports this conclusion by showing that the pits fall between particles, not on them. At very high magnification (X 400,000) this conclusion is also suggested even without stereo viewing (Figure 33).

Figure 20 illustrates the application of technique 5 (step 5) to the right and left panels of Figure 19. The figure also shows that the configuration of the spaces between E-face pits is often congruent with the shape of the particles (or aggregates of particles) that fall between the pits on the corresponding complementary P-face. In Figure 35, a system of coordinates (a) is defined by lines connecting the E-face pits (b); the particles from the complementary replica (c) are shown to superimpose on the spaces between the coordinate lines (d). Both the use of the Zeiss "blink microscope" (technique 6) and of the large mirror stereoscope (technique 7) confirmed the structural conclusions reached on the basis of the above-described analysis.

Measurements of surface densities of particles and pits for P-face and E-face of GJ

The x-y coordinates of the centers of particles and pits were digitized from reverse printed photographs at magnifications of X 510,000 - 912,000 using a Ladd_Graphic Data Analyzing System; their numbers/pm^2 of membrane fracture face were computed as previously described (Kordylewski et al., 1983, 1985; Page et al., 1983). The numbers of particles and pits for equal areas of GJ P- and E-faces were compared.

Table 1 gives the values (in number per um^2) for particles and pits measured in corresponding areas of complementary replicas. The sample consisted of four GJs from sheep cardiac Purkinje strands. Mean center-to-center nearest neighbor distances (NND), calculated from the digitized x-y coordinates of particle centers and pit centers, are also given. The table shows that the number of E-face pits exceeded the number of P-face particles in all four junctions by a factor of 1.34 to 1.51. At the same time, NND was consistently smaller for pits than for particles.

Table 1

Measurements on Complementary Replicas of Gap Junctions

Gap Junction #	Mag. ($\times 10^{-3}$)	Fracture Face Area Examined (μm^2)	Number of Particles or Pits in the area	Number/μm^2	NND*	$\frac{\text{Number of pits}/\mu m^2}{\text{Number of particles}/\mu m^2}$
1 (fig. 7)						
particles	750	.045	571	12.8×10^3	6.280	1.34
pits	750	.045	763	17.1×10^3	6.024	
2 (fig. 7)						
particles	510	.021	177	8.57×10^3	8.017	1.37
pits	510	.021	242	11.8×10^3	6.20	
3 (fig. 8)						
particles	912	.033	344	10.3×10^3	6.541	1.51
pits	912	.033	521	15.6×10^3	6.133	
4 (not shown)						
particles	760	.043	105	9.70×10^3	7.025	1.50
pits	760	.044	158	14.4×10^3	5.611	

* Mean nearest neighbor distance (Page, et al., 1983)

Origin and critique of the idea the GJ particles and pits are complementary

The notion that GJ particles and pits are complementary structures is widely accepted, as is the corollary that both lie on the axis of the cell-to-cell channel (e.g., see Peracchia, 1980, Fig. 5E). This concept does not, however, rest on extensive studies of complementary replicas. This question has not previously been examined with stereo imaging of complementary replicas, followed by superposition of carefully aligned images of the complementary fracture faces, i.e., with techniques that are considered essential for demonstrating non-complementarity. Even when complementary replication was attempted, the usual procedure has been limited to "mirror image" photographs of the complementary fracture faces (Chalcroft and Bullivant, 1970; Steere and Sommer, 1972). The idea that pits and particles might be non-complementary was considered in mouse liver GJs freeze-fractured *in situ* by Goodenough and Revel (1970), who stated that "*close examination of the serrated edge between the two views of the junctional membranes suggests that the pits correspond to some of the spaces between the particles and not to the center of the particles themselves. In favorable views, the pits closest to the*

serrated edge are seen in line with the spaces between the immediately adjacent particles of the particulate lattice. The data available at present do not indicate that the pits are openings of channels passing through the junctional membranes, but it is not possible to eliminate this suggestion." Caspar et al. (1977) studied freeze-fractured (*in situ*) mouse liver GJs in which the particle pattern was rendered more highly ordered by perfusing the livers with 0.5 M sucrose before fixing them. They found that the pattern of E-face pits could be approximately matched with (superposed on) the P-face particles, and concluded that "the order in the two faces is similar." They did not comment on the issue of complementarity of particles and pits. Their result does not prove complementarity of particles and pits; for example, appropriate translations of the pit pattern along the x- and *y*-axes would shift their location to the spaces between particles, leading the observer to infer non-complementarity. Examination of regular "crystalline" arrays of pits and particles may therefore result in ambiguous conclusions. Instead, in the present paper, the deliberately sought irregular patterns of pits and particles served as landmarks that were unequivocally matched on both faces. Based on the assumption that, in the native state of the junctions, the structures corresponding to GJ particles and pits lie on the same transmembrane axis as the cell-to-cell channel, the finding that particles are more widely spaced and less orderly than pits in freeze-fractured junctions has been attributed by other authors to plastic deformation during freeze-cleaving. This process has been thought to affect the particles more than the pits (Peracchia, 1980). There is indeed no convincing evidence for plastic deformation of membranes and proteins during freeze-cleaving (Bullivant, 1974; Sleytr and Robards, 1977). That plastic deformation may occur does not, however, explain the systematic relationship between particles and pits described at present - pits falling between particles, particles bulging behind the spaces between pits.

Apparent exceptions to this systematic relationship merit discussion.

The model in Figures 15 and 16 predicts a 1:1 ratio of pits to particles, but it has been found that, in complementary areas of complementary replicas, the number of pits significantly exceeds the number of particles. Three artifacts have been identified that may contribute to a spuriously low particle count without affecting the count of pits: (a) some particles are lost during freeze-fracture for unknown reasons; (b) two or more particles may appear to be fused and therefore be counted as a single particle, and (c) some particles may cast shadows that obscure other particles. Moreover, excessively heavy shadowing may obscure the pits. This artifact is usually readily identifiable in some areas in which the topography of the replica varies; consequently, the slope of the E-face is oriented unfavorably with respect to the angle of shadowing and the pits do not show (e.g., Figure 21).

The possible causes for the variation of numbers and shapes of pits is discussed and illustrated in Figs. 36-39. Although the angle of

unidirectional shadowing of single and double replicas is set constant (22 degrees), the varying topography of the fractured membranes plays a crucial role in a more or less distinct appearance of pits and affects their shape, also depending on the direction from which Pt/C is deposited in relation to the orientation of the hexagonal grid of pits/particles in GJ.

Nature of the pits

What are the pits? The present data indicate that they are neither, as previously thought, concavities or depressions left by pulling the particles out of the E-face. The focus of the inquiry about their nature must be on the material in the "spaces" between particles. In the model of Figures 15 and 16, the areas between the pits are seen to be tented upward, a convexity caused by the particle bulging into the back of the E-face membrane. The bulge corresponds exactly in location to its mate (the other P-face particle of the same connexon) on the complementary P-face. Shadowing reveals that the pits are the points of deepest depression in the area surrounding the particles hidden behind and bulging into the back of the E-face. A different way to express the same idea is to regard the E-face areas between pits as convex membrane casts of the underlying particles, with the E-face pits occupying the points defining the base of the cast. One possibility is that the pits are merely shadows behind the bulges.

Alternative interpretations must take into account the composition of the material between the particles. Not much is known about this question. Low-irradiation electron microscopy of negatively stained liver GJs isolated with detergents shows a large variation in the amount of stain between connexons, with little stain in a triangular region at the threefold axis (Baker et al., 1983). Peracchia and Girsch (1985) have presented preliminary evidence for filamentous bridges between particles of isolated liver GJs subjected to rotary shadowing and deep etching to the ES-surface after pulling the junctions apart with hypertonic sucrose. These filaments (1.5 - 2.2 nm thick and 1.5 nm long) were observed to join neighboring particles or to join end-to-end with other bridges. In stereo images the bridges were located at a level lower than the particle summits.

Similar connecting structures were detected in reconstructed images of isolated liver GJs studied by low dosage electron microscopy (Wrigley et al., 1984). The relationship of these as yet incompletely defined structures is speculative. The present data is confined to the location of the pits. The nature of the pits remains to be conclusively established.

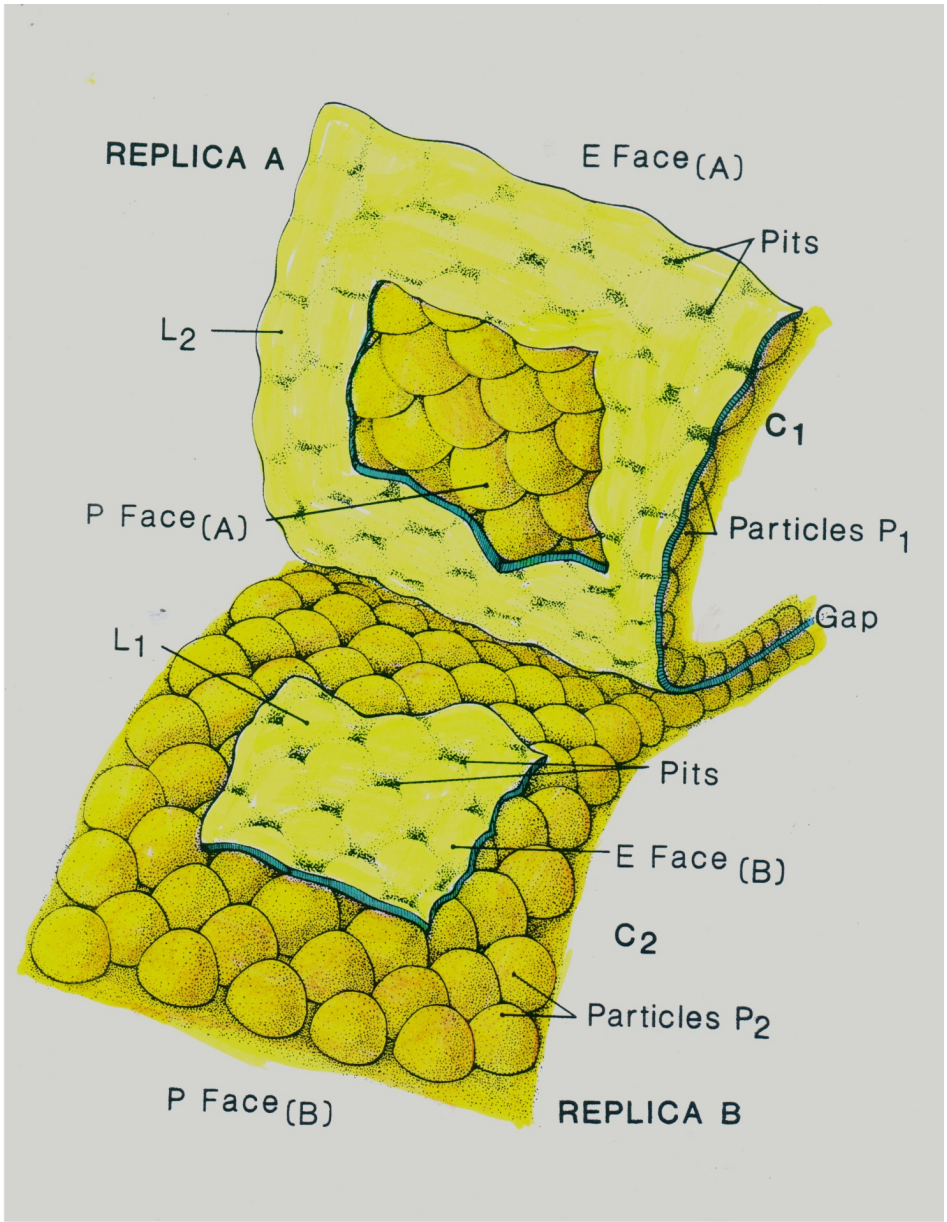

Fig. 16

Above is the same "split mattress" diagram as in Fig. 15, enhanced with color to make the relations between its complex details more clear. This 3D diagram should be studied with reference to the cross-section ("hamburger") diagram shown in Fig. 7 and also to more detailed diagrams of the spatial organization of GJ in Fig 17.

Seen in the back of the 3D model presented in Fig. 16, the intact "mattress" is composed of two sets of "oranges". The "oranges" represent GJ particles of the unsplit membrane. The upper set belongs to cell C1, while the lower set belongs to cell C2. In the native intact junction before splitting, the "oranges" are hexagonally arrayed in two layers which are separated by (or rather "glued together" with) a layer of "lemon frosting" (L). Within this layer L lies the intracellular space, narrowed here to a characteristic "gap" known from the cross-sectioned samples of GJs. The layer L is apparently composed of both external lipid bilayers of the neighboring cells C1 and C2, which adhere tightly to each other in the intact GJ.

When the membrane "mattress" is being split during the FF procedure (shown in the foreground), the orange layers become pulled apart into lower and upper portions of the split sample. At that time the "frosting" layer L usually becomes torn into patches: L1 and L2. Some patches (L1) stay with the base C2, while others (L2) travel with the lifted cell C1. This process cannot be controlled because the FF crack proceeds at random. In some samples the entire not-torn-into-patches layer L travels with C1 (or C2), appearing in the replica as the pitted surface (E-face) in the entire area of the GJ.

As a result of FF splitting, in the replica A the pitted surface of the layer L exposes the inner site of the membrane (m2) which originally belonged to the lower cell C2. In the replica B the inner site (L1) of the opposite membrane (m1) of the upper cell (C1) shows as the E-face.

For reasons never explained so far, the actual "gap" of the GJ never shows in the FF samples. Marked as the "blue ham" in the "sandwich" in Fig. 7, the intact gap runs between two halves of the adhering membranes (m1 and m2) of the respective cells (C1 and C2). The crack never passes along the gap itself. Therefore the external surfaces of the membranes (lipid bilayers) are never exposed. The FF crack always runs between the bilayers of the membranes, thus the intercellular gap is contained in the step (blue) where the fracture plane passes down from E-face to P-face (see also diagrams in Figs. 7 and 17). Such a step is only present in replicas that share E-Faces and P faces next to each other; in those images that show “clean” faces split completely into exclusively

particulate (P) or pitted (E) fields over the entire area of GJ such step is not seen, because in such cases the fracture crossed from E-face to P-face outside the GJ area.

The blue edge of the of the patches of the frosting corresponds to the blue space in the “hamburger” diagram explained before. The frosting patch L1 removed from the “window” is complementary with the “window” frame. This patch, as well as the rest of the “frosting” contains the “gap”, which is nothing else but the intercellular space tightly narrowed in the GJ region. In the intact junction before fracturing, the patch L1 is continuous with its counterpart L2. After fracturing the reverse side of the same “frosting” layer is seen, lifted with the upper set of “oranges”, adhering to them above. The lower half of the “split mattress” represents one replica; the upper half represents the other one, which is complementary to its mate.

The “lemon frosting” layer is densely marked by the regular pattern of pits, which are obviously aligned with the spaces between the underlying particles, and are not located on their tops. The pits show as evident depressions of the E-face layer between the particles, while the particles manifest themselves as distinct bulges as if they were wrapped with the E-face layer of “lemon frosting”. These pits can in no way be aligned with the tops of the particles, therefore they cannot be marking the “scars” after removing the corresponding set of particles of the other cell. Assuming that the channels are penetrating the centers of the particles perpendicularly to the particle bases, in no way can the pits be any part of such channels. Pits cannot be aligned with those particle axes because they are clearly located outside the particles, in the spaces between the particles.

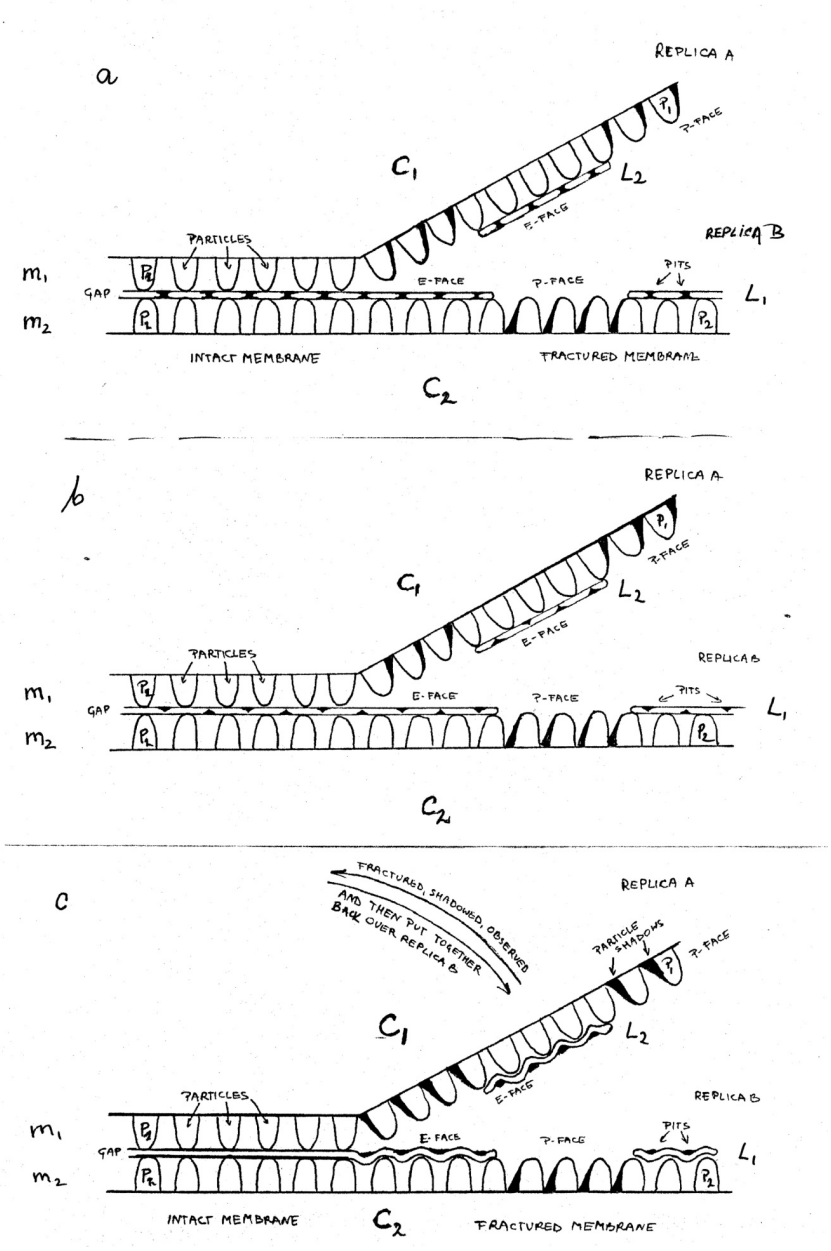

Fig. 17

This diagram (Fig. 17) shows a side view of the "split mattress" model in Figs. 15 and 16 in cross section, similar to the "hamburger diagram" in Fig. 7. Here the structural details (particles and pits) of both replicated membranes (m_1 and m_2) are included. The possible origin of pits is discussed and illustrated in three slightly different panels (a, b, c). In each panel the pits are correctly located between the particles, as they appear in all my GJ electron micrographs, both single image and 3D (Figs. 18-34, 42, 44-48). All three possible options illustrated in Fig. 17 show that the gap, which is contained between two outer lipid monolayers of the membranes (m_1 and m_2) of joined cells C_1 and C_2, after fracturing always stays with the opposite cell to the one showing particulate P-face covered the "frosting" of the outer layer, which in the replicas shows as pitted E-face. Particles (and P-face that carries them) are exposed where the gap-containing "frosting" layer travels with the opposite cell, like in the "window" shown in the "mattress" diagram in Figs. 15 and 16. I suggest that pits (seen in the E-faces) may either result from preexisting openings in the "frosting" (upper panel a in Fig. 17), or they may show some asymmetry in distribution (medium panel b), or they may result from undulations of the E-face ("frosting layer") "molded" on the set of particles on which the layer rests (bottom panel c). The third option is closest to the real situation observed in my 3D images of GJ E-Faces in complementary replicas.

EM images of complementary replicas

Fig. 18

Two electron micrographs in Fig. 18 show complementary replicas of the same freeze-fractured GJ in a sheep cardiac Purkinje fiber. The images were oriented to display the symmetry of the complementary details contained in both replicas. Although both images are different, the symmetric details can be identified on both sides. This is a non-stereo image. Both micrographs were mounted to show symmetric analogy of the particulate P-face (mostly in the left picture) and pitted E-face (mostly in the right). The symmetry line divides these two images in the middle of this figure, as if the left and right pictures were consecutive pages of a book. The structural details of both images complemented each other before the book was open, i.e., before the GJ has been split by FF and shadowed. The left panel is made up predominantly of the particulate P-face of the membrane; the right panel shows the pitted complementary E-face. Numerous caveolae present in the upper part of the micrographs also display symmetric complementarity, as if the replicas were impressed in each other. This and all subsequent electron micrographs have been double-printed so that shadows appear black. The dark bottom of the right panel is due to an artifact of the

right replica: apparently the replica was torn along the waved line and its torn away lower section has been detached. This is more pronounced in Fig. 19 (bottom) where the wavy configuration of the fractured membranes is better seen in the stereo views of the same two replicas. The original magnification at which these images were photographed is 50,000 x.

Superimposing 3D EM images

In the following paragraphs, I will discuss in detail my method of using the 3D images of the fine structure of the replicated GJs and illustrate my description with the original images.

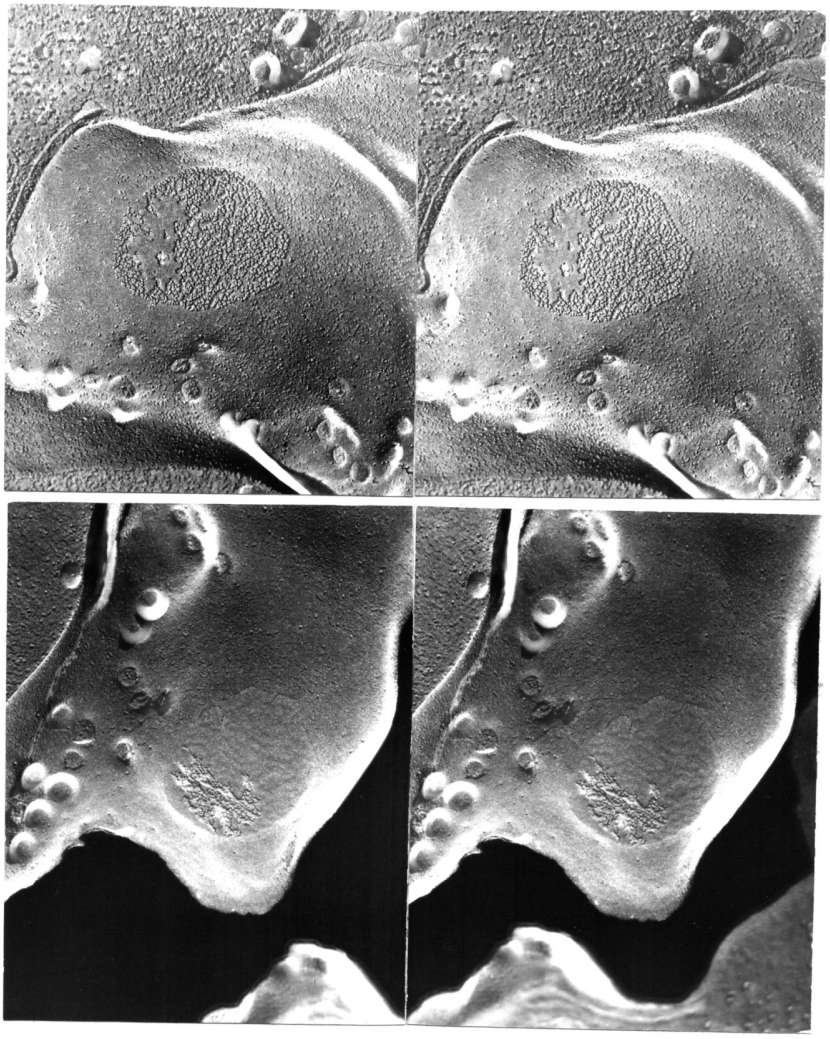

Fig. 19

Above is the set of two stereo pairs of the GJs shown in Fig. 18. This set, as well as those in images of other GJs below (21, 28, 29, 30, 42, 45, 46), should be looked at with a stereo viewer (or with the X-3D method of crossing naked eyes) to bring out the layered structure of the junction and to see how the junction splits to produce complementary replicas. The upper stereo pair shows mainly the particulate P-face of the membrane; the lower

stereo pair shows mainly the E-face. The large, branched, particle-free area in the middle of the upper stereo pair is a patch of the E-face (layer L in Figures 15 and 16). This layer covers the particles underneath it. A similarly shaped opening ("window") through which P-face particles are visible in the E-face can be seen in the complementary replica (the stereo pair in the lower panel). Such stereo views show that these particles lie in a different plane than that of the P-face particles in the upper panel. Although for the stereo effect the photographs could not be oriented to the ideal position to show the symmetry of the details in the P- and E-faces, the horizontal white bar dividing both stereo pairs approximately represents the symmetry line, similar to the vertical line dividing the single non-stereo images of the same replicas in the previous figure (Fig. 18). Original magnification 50,000 x.

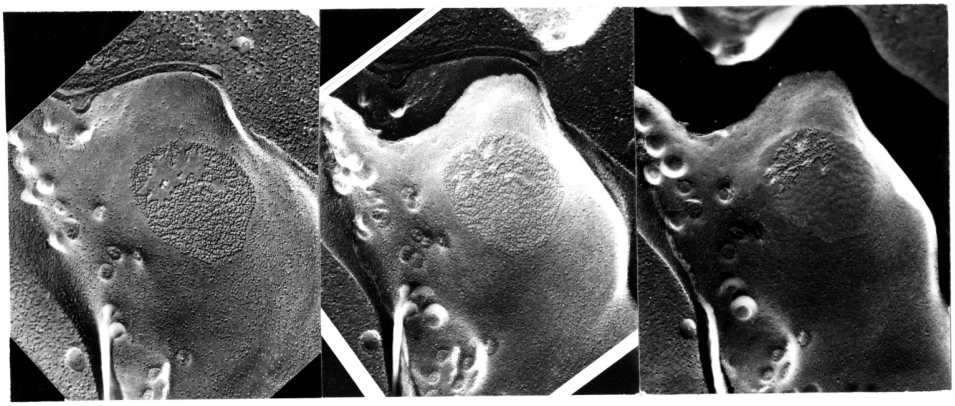

Fig. 20

This panel contains images of complementary replicas of the same GJ as in previous Figs. 18 and 19, displayed here as a sequence of three photographs. These are two stereo images arrayed as in step 4 of the diagram in Fig. 7. In this montage of stereo-pairs, the central panel contains images of E-and P faces of the same GJ superimposed on each other. The left and central panels constitute the stereo image of the P-face, the right and central panels constitutes the stereo pair of the E-face. By using the stereo viewer (or X-3D method) and shifting it from one pair to the other, the observer can alternate from one stereo image to the other to see that superimposition causes the E-face pits to fall in between the complementary

P-face particles. It is striking that the array of pits fits well the pattern of spaces between the particles, not the particles themselves. Furthermore, the particle pattern on the P-face is traceable on the E-face; for example, the small, particle-free oval area is also detectable under the E-face. This clearly indicates that the missing particles were not lost in the FF process, but were absent in this area of the GJ even before it was split. Alternate stereo viewing of the right and left stereo pairs shows that, in favorable areas as on the right, the branched pattern of spaces between E-face pits is exactly filled with particles. The similar patterns of particle clusters can also be identified on the pitted areas. Original magnification 50,000 x.

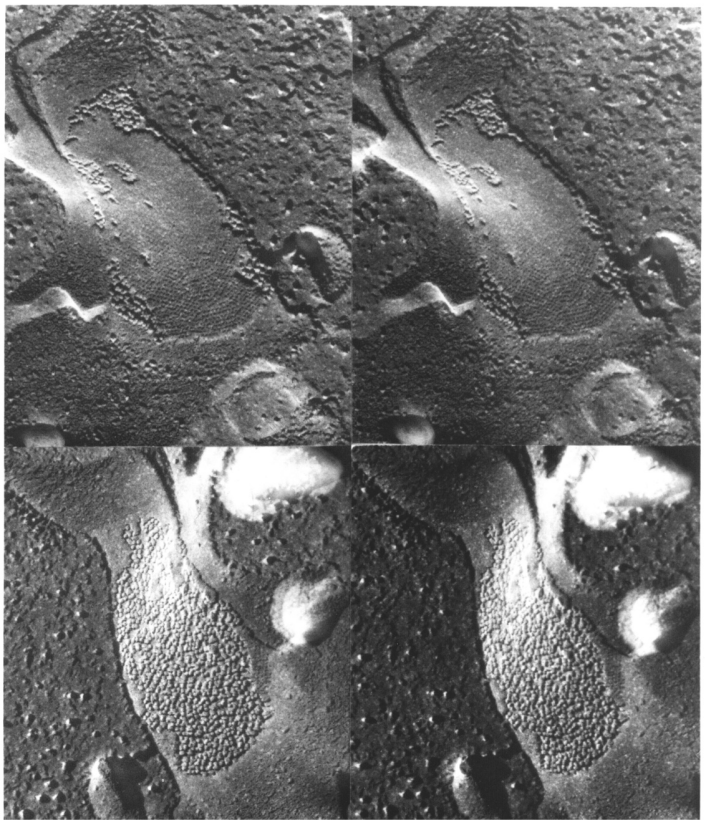

Fig. 21

This is a similar set of two stereo images of complementary faces of a GJ which, on stereo viewing, displays marked curvature of its surface. A slight difference in the slope produces a difference in the shadowing angle that causes the pits to disappear in the upper region of the GJ, whereas they are well visualized in the lower part of the patch of the membrane. The clear outlines of the shapes of the patches of the E-face portions which appear on both complementary replicas facilitate identification of complementary areas on P- and E-faces. The most convenient areas for the purposes of such identification are those so small that they contain few particles or pits; such areas are suitable for matching at high magnification. The identifying landmarks are the structural details surrounding the areas to be matched, e.g., the edges of fractured membranes or the structures in the cytoplasm. Original magnification 100,000 x.

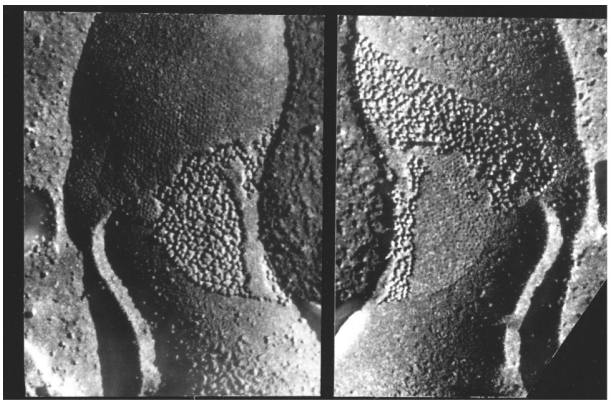

Fig. 22

This is yet another GJ split into pitted E-face and particulate P-face, seen in two complementary replicas. The images of the replicas were mounted next to each other to demonstrate symmetry of the complementary details against the central vertical dark line. Original magnification 100,000 x.

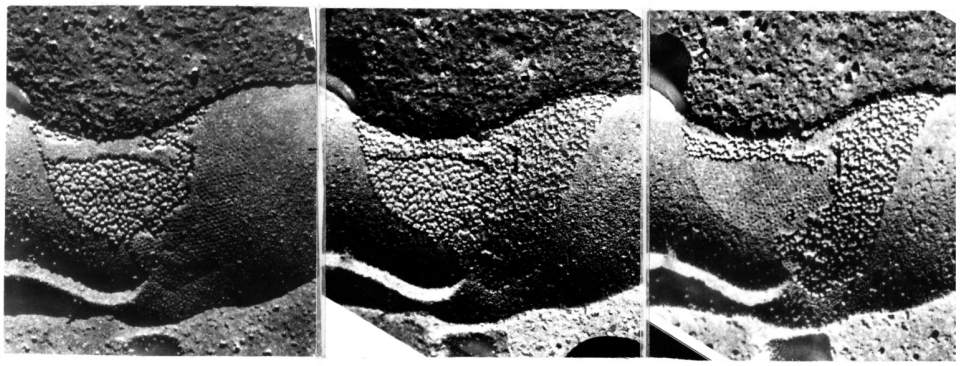

Fig. 23

The images of the same complementary replicas (Fig. 22) were rotated here by 90 degrees and mounted as a threefold panel to show the complementarity of pits with the spaces between the particles. As in previous three-panel montage (Fig. 20), this is a sequence of two stereo pairs combined in a threefold panel for stereo viewing of complementary replicas mounted as explained in the Fig. 7 (step 4). These two stereo images are to be viewed alternately with a stereo viewer (or X-3D method). At a higher magnification the location of pits in the spaces between particles is well demonstrated. The middle picture contains two combined images: the right member of the left stereo-pair printed together with the left member of the right stereo-pair. In this way two stereo-pairs are overlapping in the middle to show the relations of pits and particles. Because the middle panel contains superimposed 3D images of the E- and P-faces of the same GJ put back together, it gives the idea of the original relations of the structural details in the intact GJ, before it was split and shadowed. The GJ observed in this unique way in 3D becomes filled with the particles from both faces, while at the same time it contains all the pits from both left and right pair of pictures. Such views have never been used before. They allowed me to verify the conclusion that E face pits usually fall in the spaces between the particles of F-face. Original magnification 100,000 x.

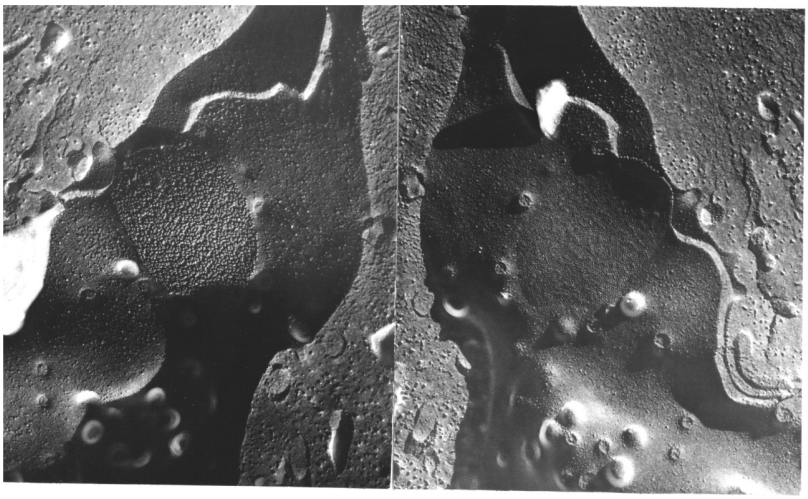

Fig. 24

Oval GJ is shown above in two low power images mounted in the "open book" manner to show the symmetry of the surrounding cellular details. Triangular shapes in the upper left corner in the left image and upper right corner in the right image represent cross fractured cytoplasm (C_1). Abundance of "particles" seen in this region results from cross-fractured filaments and tubules running across the fracture plane near the outer cell membrane. As explained in the "hamburger" diagram, the fracture follows the plane of one membrane (m_1), crosses the "gap" and exposes the interior of the other membrane (m_2) of cell C_2, in which pits of the GJ are seen in the right replica, while the corresponding particulate area is seen in the left replica. Some caveolae are seen outside the oval outline of GJ in the form of circular trunks of the broken off necks or as shallow depressions. This is not a stereo image. Spatial relations between the structural details and the general three dimensional topography of the viewed area is better seen in the 3D images in the stereo pairs shown in Figs. 28-30 below. When inspected with 3D spectacles (or X-3D viewing method), the flat single image turns into a very spectacular three dimensional scene.

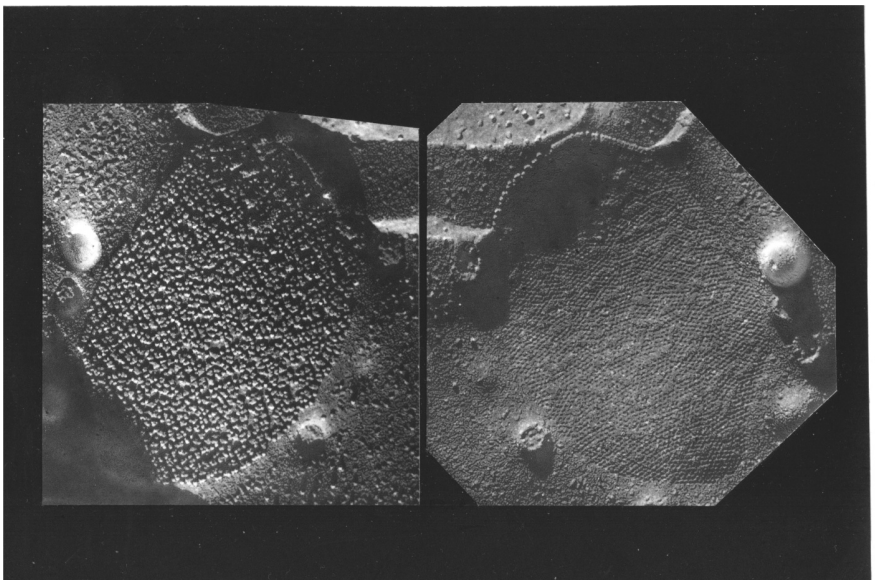

Fig. 25

These are non-stereo images of the same GJ as in the previous figure, oriented to show the symmetry of the analogical details. The oval outline of the split GJ manifests itself similarly on both faces: the particulate P-face is seen in the left panel, the pitted E-face is seen on the right. Different orientation of the images of the samples causes the shadows (fixed permanently in the replica) to be redirected which may help in better understanding of elevations and depressions in the specimen. When in the image shadows are directed in an oblique manner from upper right or left down, they resemble the natural situation in which light comes from above casting shadows down. If the images are mounted upside down so that shadows are directed up, they may create the illusion of the reversal of elevations and depressions: the images of pits may look as if they are sticking up, and images of particles may seem to appear concave. The same applies to the prints of the original negatives, in which the shadows would appear white, rather than dark. Therefore, for the purpose of easier understanding of elevations and depressions in the replicas, their images were always double-printed to reverse the shadows seen in the original negative films taken in the EM as dark spots. Out of each original negative film (with dark shadows) a secondary contact negative was produced, to show the shadows white. This secondary negative was then contact printed on photographic paper, without magnifying the image, to maintain the original magnification (1:1). Thus, the shadows in the final prints always showdark, as in the original films taken with EM.

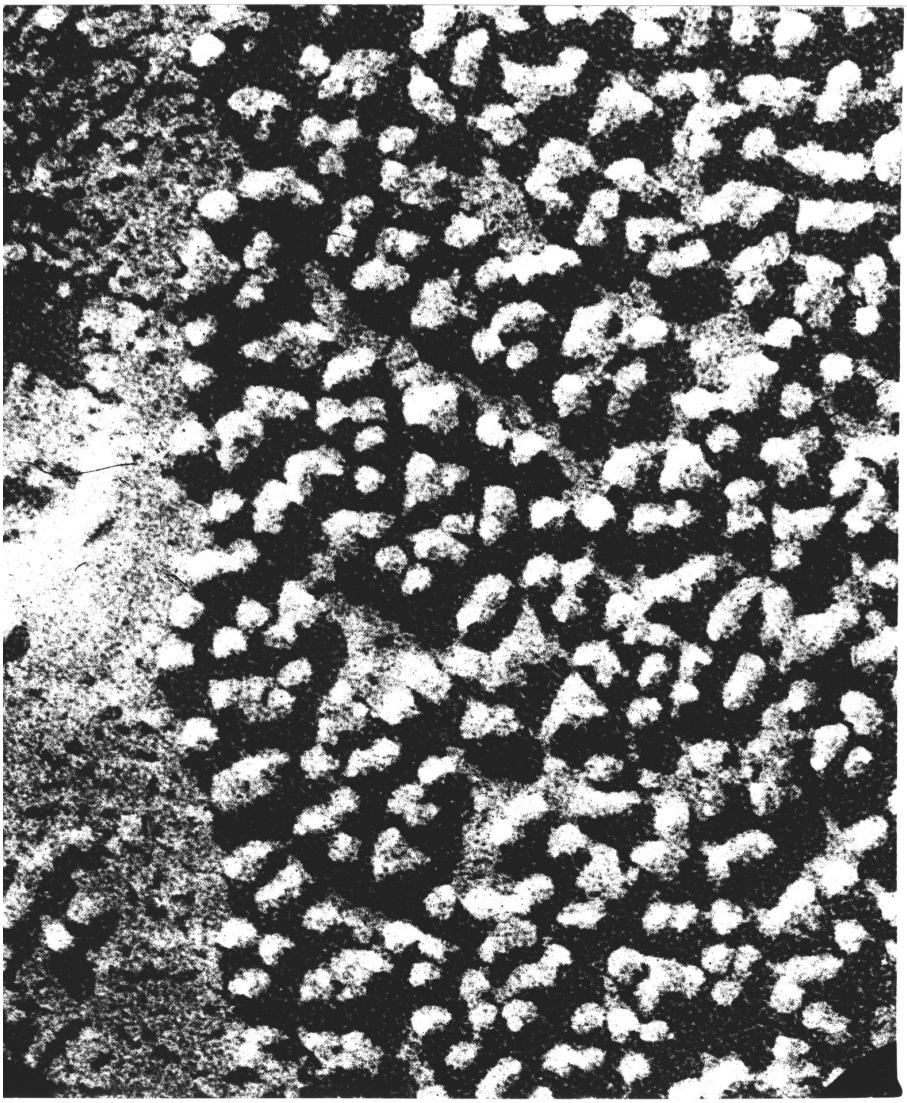

Fig. 26

Fig. 27

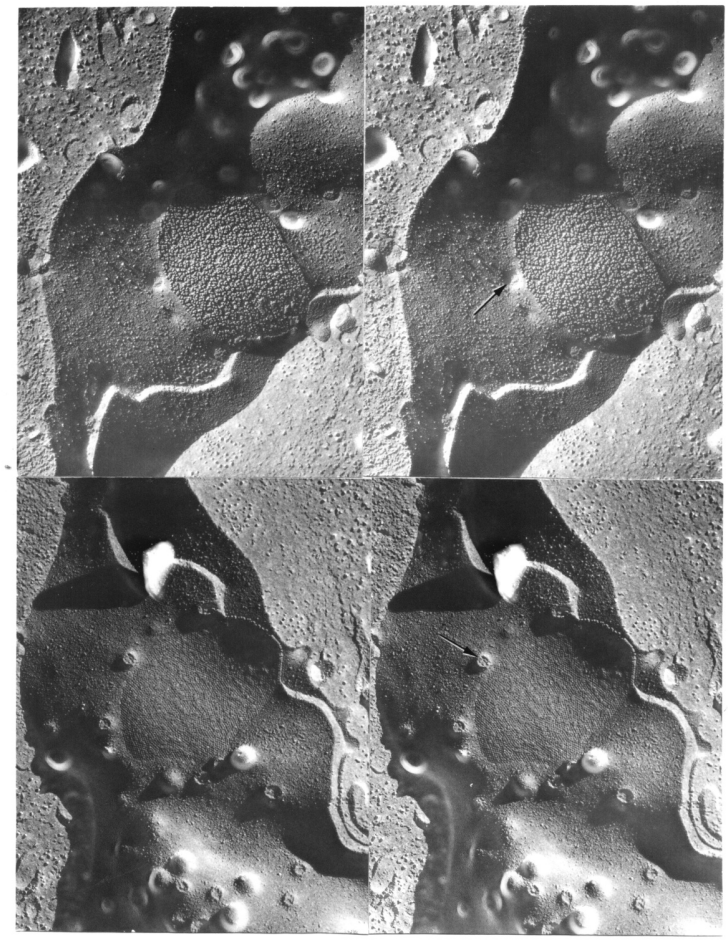

Fig. 28

Above are two stereo pairs of complementary replicas of the same GJ. They were mounted so as to display the symmetry of their structural details on both surfaces (particulate P-face in the upper pair and pitted E-face in the lower pair) along the horizontal line of symmetry dividing both stereo pairs. This GJ has split in such a way that only the pitted E-face appears on one replica (lower stereopair), while only P-face particles appear on the other replica (upper stereopair). In this GJ replica no "windows" of the "lemon frosting layer" were created (which were explained in the "matress diagram" in Figs. 15 and 16).

All “frosting” in the form of a continuous E-face covering the entire oval GJ travelled with the lower replica, while the upper set of pictures shows the entire oval of GJ covered exclusively with P-face particles. A closer look at the stereo view of the E-face clearly reveals the presence of a second layer of particles showing under the E-face of the lower stereo pair that form a pattern analogous to that displayed by the first set of particles exposed on P-face. While P-face particles belong to the upper cell, this other set of particles covered with E-face “frosting” belongs to the lower cell. This other layer of particles manifests its presence by bulges in the area between pits. The arrows point to the extra-junctional landmark, a caveolar neck, which is also present in next figures at higher magnification. The caveolae or their neck outlines show convex profiles in one 3D image whereas they are complementarily concave in the other. Original magnification of the images here is 50,000 x.

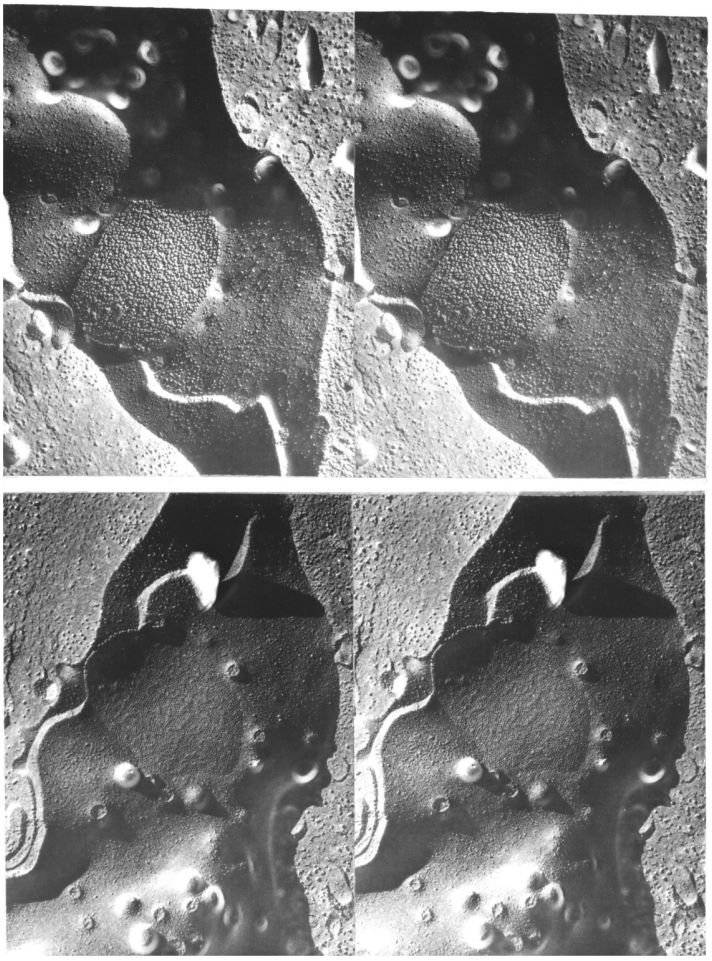

Fig. 29

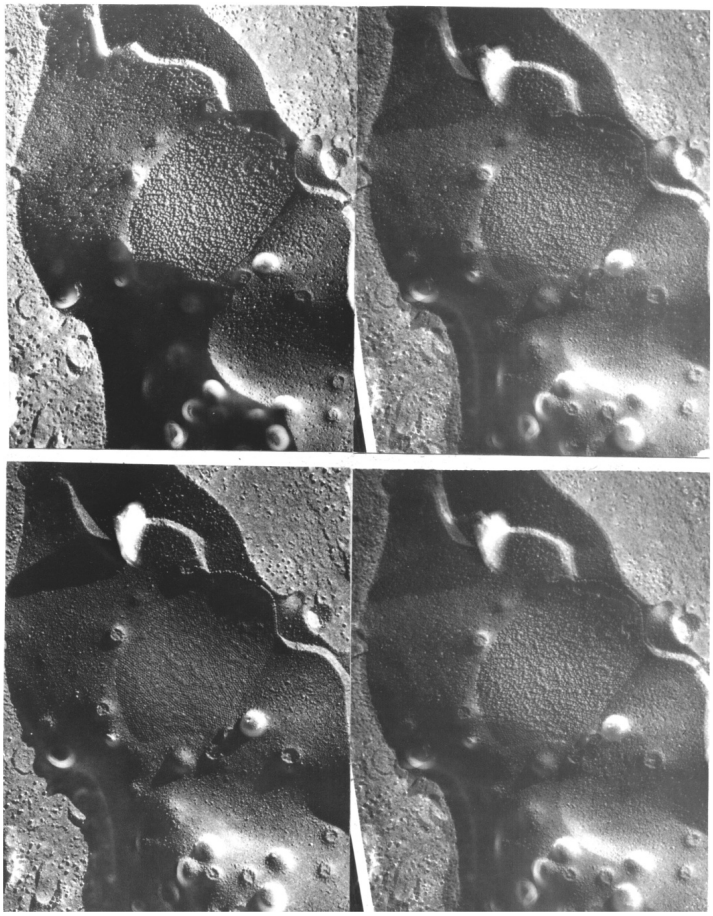

Fig. 30

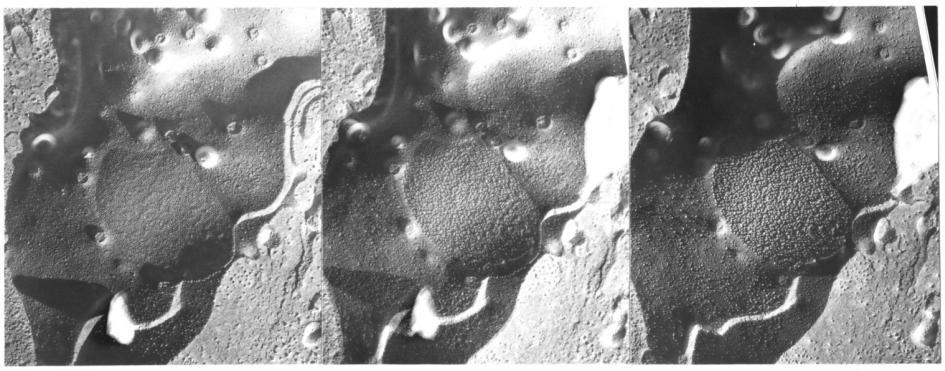

Fig. 31

The above photograph is a triple array montage of the images of GJ shown in the previous four figures, mounted for stereo viewing as in the previous threefold panels (Figs. 20 and 23). In the central area of the GJ, where the alignment of both stereo images is good, it is evident that the pits fall into the spaces between particles, not on them. Original magnification X 50,000.

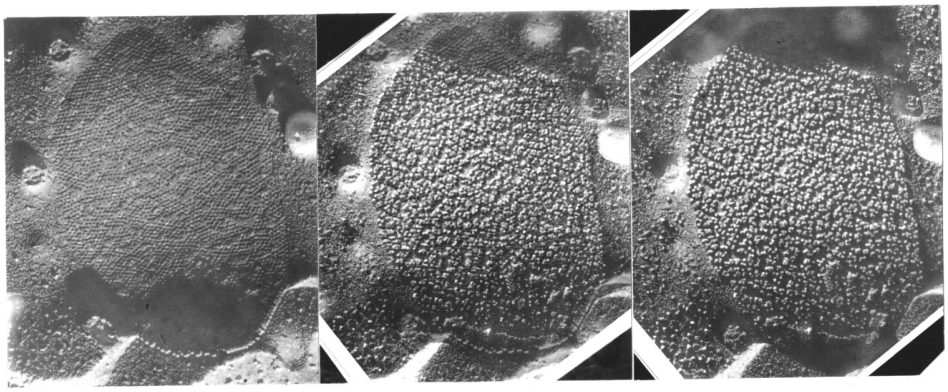

Fig. 32

A higher magnification of the array shown in the previous figure. Original magnification X 100,000.

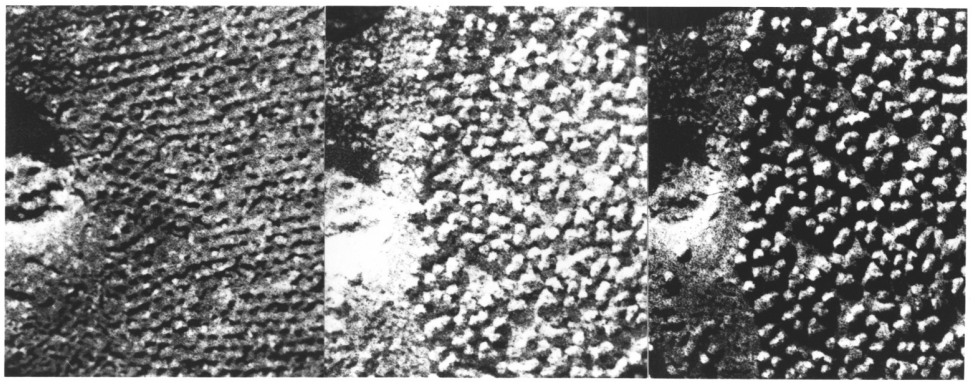

Fig. 33

A greatly magnified portion of the GJ shown in previous three figures. This is not a stereo set, although the two complementary faces (right and left panels) were combined to produce the central panel. Some of the particles on the particulate surface (right) are missing, while others are obscured by heavy shadowing. The array of pits on the pitted surface (left) is more regular than the particle pattern (right). The middle panel shows how well the features of the right and left panels can be matched. These images should be compared with the tracings and "maps" in the next figures below (Figs. 34 and 35). Near the left margin of the GJ, a fragment of the caveola (indicated by an arrow in one of the previous low power images) is located next to an unusual triangular pattern of array of pits and particles. This pattern can be used to compare the locations of the corresponding particles and pits here and also in all three panels of the previous lower power 3D image of the same replicas. Such comparisons show undoubtedly that in the superimposed images (which correspond to the relations in GJ before FF splitting) pits fall between the particles. Additionally, one can note here that some of the particles on the P-face are missing, while their counterparts (seen as distinct bulges on the E-face) are in place. Original magnification X 400,000.

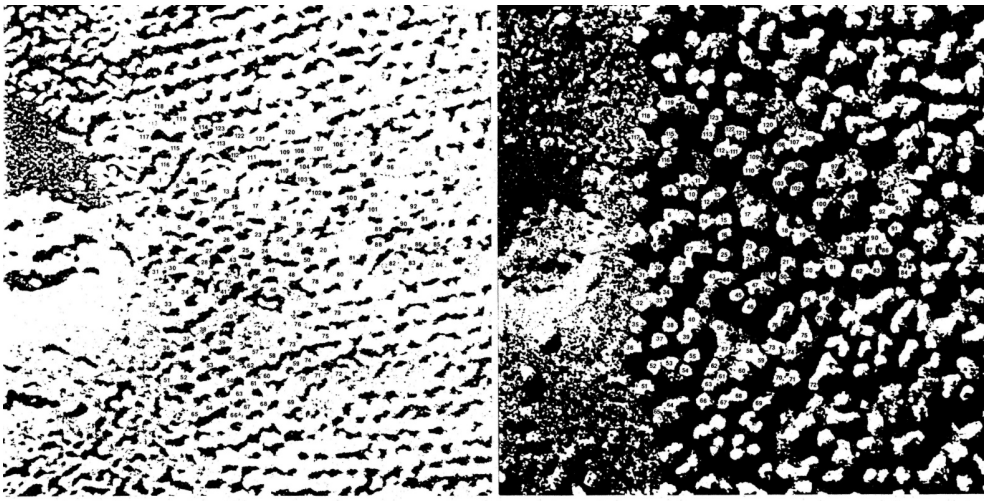

Fig. 34

These are high contrast, enlarged reproductions of nearly the same areas as in the previous figure. They were made with a copier and enlarger of the right and left panels of the previous triple panel figure. Here the right panel shows a "map" made by numbering the particles. Most of the individual particles present in this field have been assigned consecutive numbers. The left panel shows the areas between the pits corresponding to the numbered particles on the right. Particles of the other cell membrane, corresponding to the ones on right, are located under these areas, while pits are seen in the spaces between them.

This figure demonstrates that the network of pits (E-face, left) cannot be matched with the particle tops (P-face, right). The pits in the left panel rather form a grid that delineates the numbered spaces, which resemble the distribution pattern of the particles in the right panel. Most of the spaces can be matched with the same numbers assigned to each particle. The whole grid of spaces of the dark grid of pits fits the particles, while the pits fall in the spaces between the particles in the right panel.

The outline of a caveola (shown by an arrow in previous stereo images of the same GJ and by dotted circle in Fig. 35) is evident at the left margin of both panels and served as a landmark helpful in identifying complementary areas in the P- and the E-faces of these two complementary replicas.

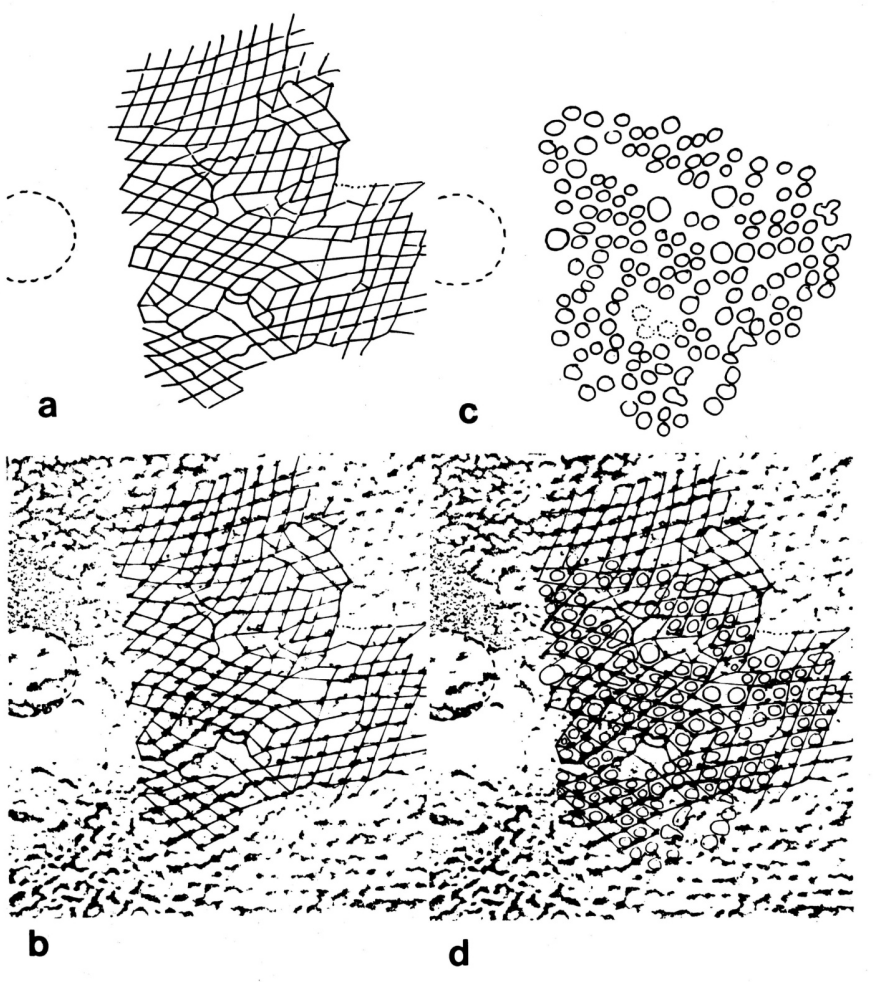

Fig. 35

These four diagrams (a, b, c, d) show the steps in the procedure for matching the structural features of the complementary gap junctional E-face and P-face shown in Figs. 29 through 34 (see Technique 5). The dotted circle indicates the location of the caveolar neck which was helpful in identifying and aligning these complementary areas of the P- and the E-faces (see Fig. 34).

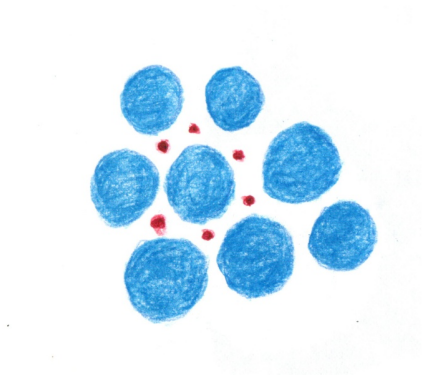

Fig. 36

This diagram illustrates that each particle (blue) in a hexagonal array shares two possible locations of the nearest pits (red) with each of the neighboring particles. This makes six possible locations of pits around each particle. In reality, in the replicas all pits do not always show well in every location, for the reasons discussed in captions to Figs. 37-39.

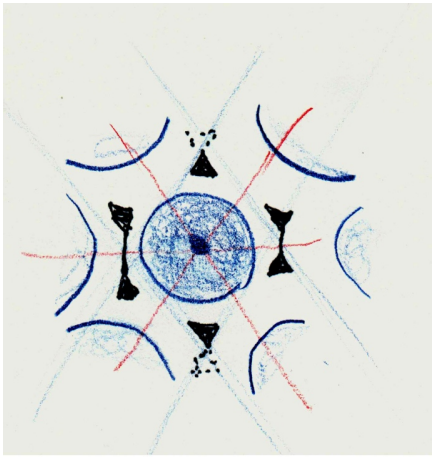

Fig. 37

This diagram illustrates why the number of pits actually observed is smaller than the anticipated 6 per particle, resulting from the location of the pits in the hexagonal grid. Some pits may show only partially (triangular marks), while others may fuse with the neighbor displaying “bow-tie” shape counted as one pit. “Bow-tie” pits are frequently seen in the spaces between the P-face particles in the E-faces of the replicated FF membranes, some are even further fused with their neighbors to form an approximately rhomboid net.

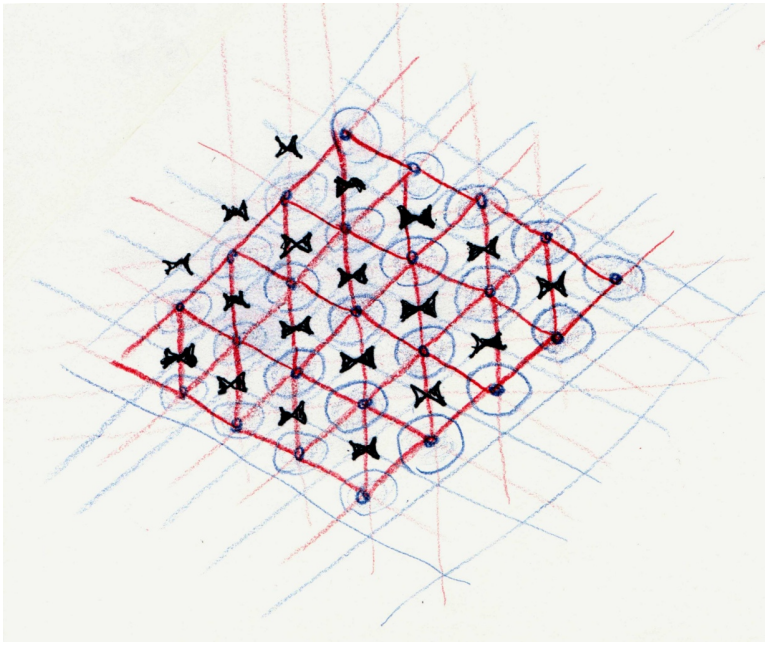

Fig. 38

The diagram in Fig. 38 shows how the hexagonal array of particles (blue) is related to the rhomboid grid (red) of pits (black) in the images of complementary areas of P- and E-faces of the membrane superimposed on each other. The "bow-tie" shapes of particles due to fusion of some pits cause the number of pits to be reduced to about 4 per particle. This model relates to the numeric data in Table 1. However, the varying number of pits per particle depends also on other factors which affect how distinct a particle shows: (1) the degree of steepness of the background membrane on which the particles are sitting and (2) the direction of shadowing in relation to the orientation of the hexagonal grid, the number of fused and/or invisible pits may vary and differ from expected based on this diagram (See Figure 39).

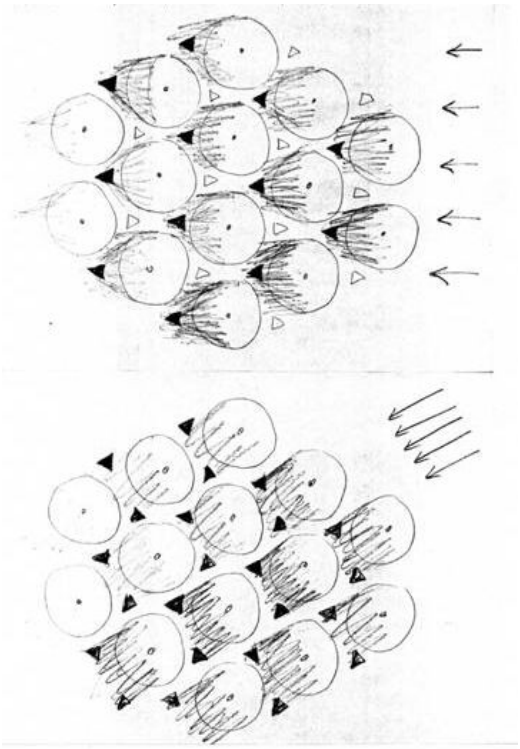

Fig. 39

This diagram illustrates why the number of pits per particle may vary depending on the direction of shadowing (arrows) in relation to the orientation of the hexagonal grid of pits and particles. Pits are marked as dark triangles (when shadowed) or open triangles, when they happen to be positioned in front of a bulge of a particle (upper diagram) and become indistinct because they were totally filled with Pt/C deposits. In reality, in the replicas a range of situations between those illustrated in both panels is found due to the varying angle of shadowing. The undulations of the membranes may cause the standard shadowing angle set at the Balzer's apparatus vary, depending on the degree of steepness of the slopes on which the particles are sitting. Deeper pits, or those obscured by a particle, will show darker and will be more likely to appear fused with a neighboring pit, than shallow pits located in front of a bulge of a particle.

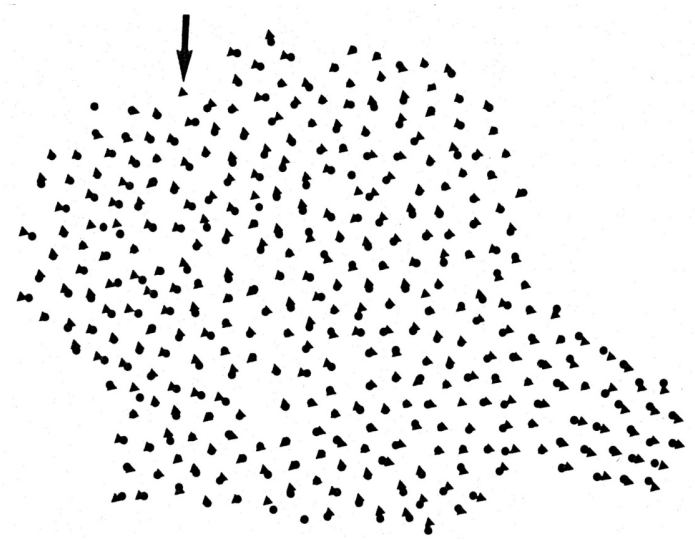

Fig. 40

In Fig. 40 the tracing of superimposed pits and particle tops is shown after DeMaziere et.al. (1987). Despite the evident mismatch shown in this diagram, these authors attributed differences in particle and pit numbers and distribution to possible “plastic deformation”, clumping of particles, and other artifacts. However, 3D imaging was not used in their study to make this graph and therefore incorrect conclusion was drawn after single flat images of pitted and particulate faces were superimposed. To show the anticipated complementarity, an attempt was made to align the marks of pits (triangles) with the marks of particles (dots), exactly as illustrated in my model of a mismatch in Fig. 70. The interpretation of this diagram (Fig. 40) leading to the incorrect conclusion was done without considering the complex issues explained in Fig. 39. According to my observations, a possible case when only one pit is seen for each particle results from one of many possible orientations of the shadowing direction (Fig. 39). Pit/particle ratio 1:1 is just one of many possible options resulting from the orientation of shadowing. For the same reason the numeric data of DeMaziere et al. (1987), which showed approximately 1:1 ratio of the number of particles and pits in the complementary replicas, are different from my data, which were gathered through 3D studies of the complementary replicas shadowed at various angles, and were based on better understanding of the nature and appearance of pits (Table 1).

Models based on the data obtained with functional, physiological, molecular and biochemical methods are not necessarily well representing the real structures because they are not based on solid morphological studies. Such models may be far from representing the real structure, as seen with

the morphological methods, therefore they may be oversimplified or incorrect. Because they are widely used, these models may contain some misinterpretations that are hard to prove to be wrong, against common beliefs. The GJ model in which the concept of complementarity of pits and particles is widely accepted may be a good example of such a situation.

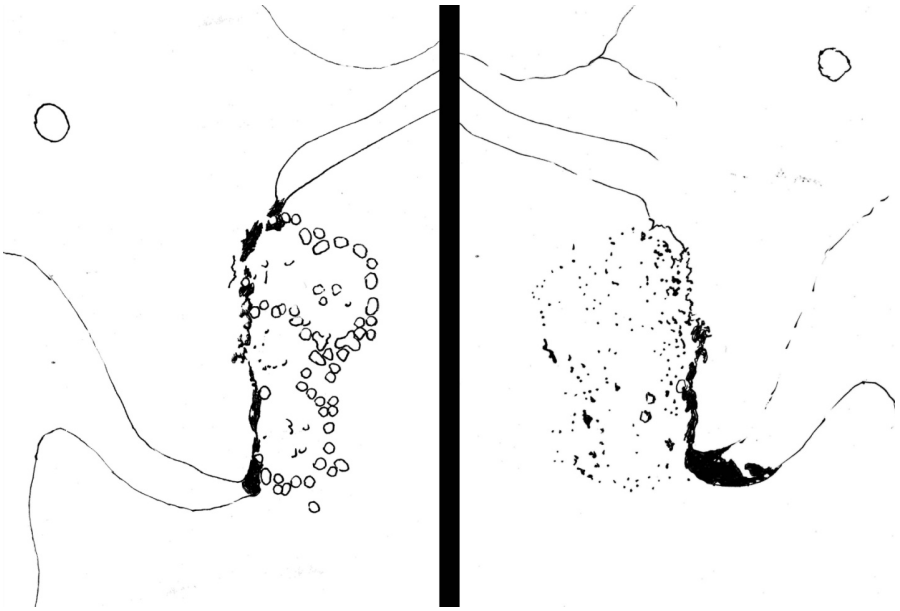

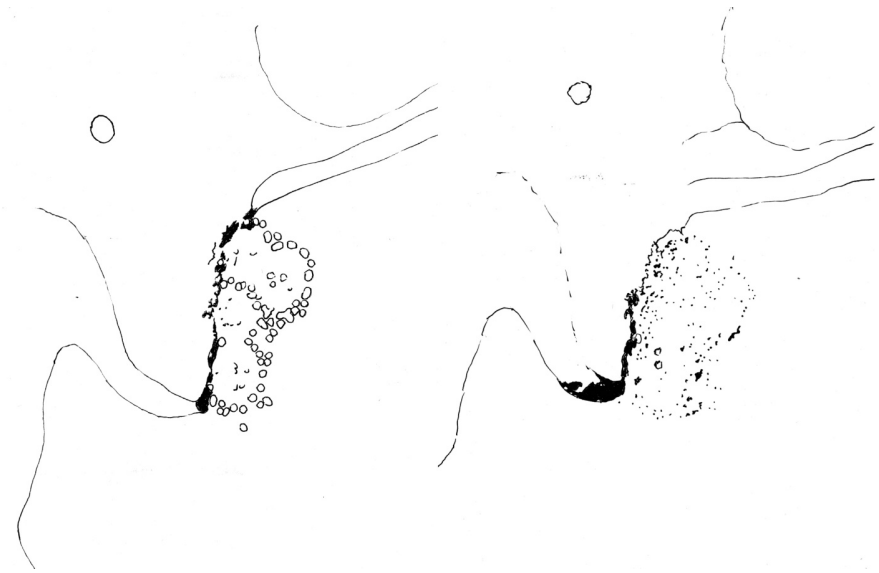

Fig. 41

The two sets of drawings in Fig. 41 show the tracings taken from the original negatives of the same GJ in the frog. The tracings were made with a Nikon projection Microscope (Fig. 6). The upper panel shows the GJ in the open book orientation, the particulate P-face (left) and pitted E-face (right), to show the symmetric feature of the complementary areas. In the lower panel the right tracing has been flip-flopped to show the analogy of the complementary areas displayed parallely. Such two tracings can be superimposed to find the exact match of the split structures (see Figures 35, 43 and 49). More numerous E-face pits (right panels) than P-face particles (left panels) can be matched with the spaces between the particles traced on the E-face (compare with the cartoons in Fig. 14)

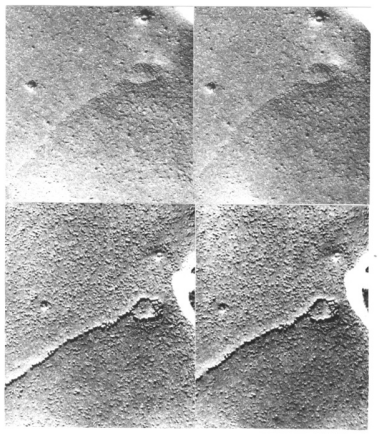

Fig.42

Two stereo images of the same frog GJ in complementary replicas are shown in parallel display (as step 3 in Fig. 7). Three zones of particle and pit arrays are distinct: linear, circular and hexagonal. Similar (complementary) patterns and zones can be identified in these stereo images of both faces of the same GJ: the pitted E-face (upper pair) and the particulate P-face (lower panel). The tracing of this GJ is shown in Fig. 43.

Fig. 43

Tracings of the frog GJ shown in Fig. 42. The upper drawing shows the pitted area in E-face and the medium drawing shows the particulate P-face of the same GJ split into complementary replicas. The bottom panel is a composite of both previous panels. It shows the best fit of particles and pits when their images were superimposed. The possible situations resulting in different appearance and the number of pits per particle discussed in Figs. 36-39 are distinct in the zone showing hexagonal array on the right.

The next five figures show electron micrographs of the same small GJ in the replica of chick cardiac membrane. The pictures are displayed in a similar way as before for sheep and frog GJs to illustrate the same conclusion: pits do not match particles the way the current common model suggests.

Fig. 44. Symmetric display of P-face (left) and E-face (right).

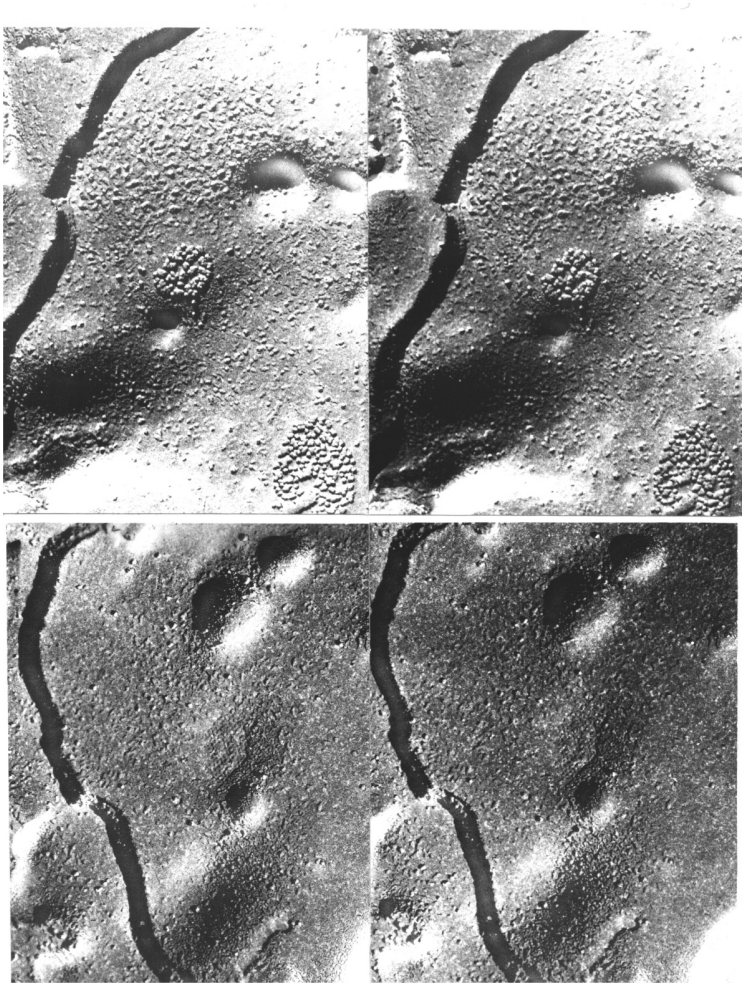

Fig. 45. Nearly parallel display of stereo views of P-face (upper pair) and E-face (bottom pair) of the same GJ.

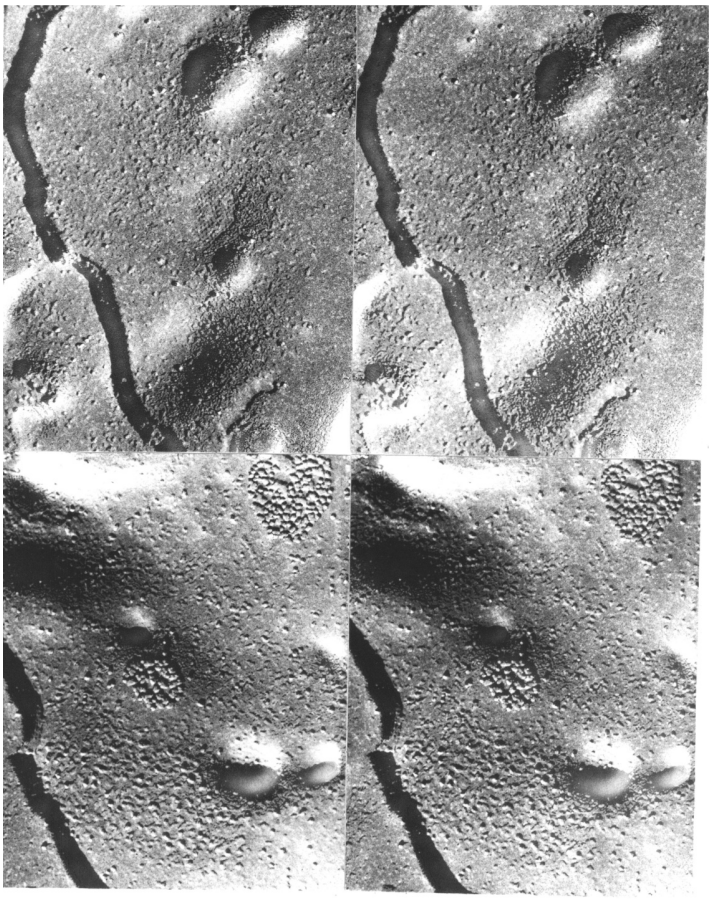

Fig. 46. The same stereo images in near symmetric display against the horizontal line dividing both pairs.

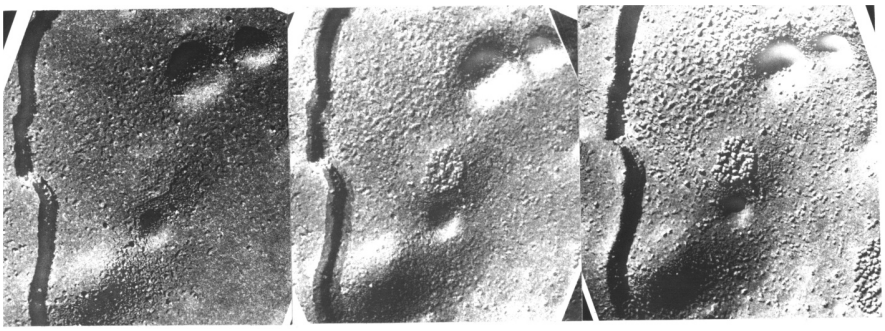

Fig. 47. The same chick GJ as in Figs. 44-46 shown in the threefold overlapping panel of two sets of stereo images: of the E-face (left pair) and the P-face (right pair) partially superimposed on each other in the center. The central photograph contains both images precisely aligned to show the complementarity of pits with the spaces between particles, as explained in Fig. 7 (step 4). Although a stereo viewer (Fig. 5) could be used to see this in 3D, the best 3D effect can be obtained using X-3D viewing method with naked eyes crossed, as in viewing popular “Magic Eye” images.

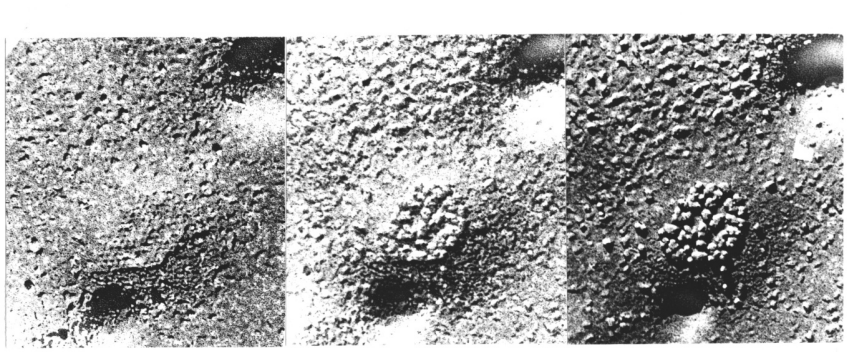

Fig. 48. Structural details of the same GJ shown as in Fig. 47.

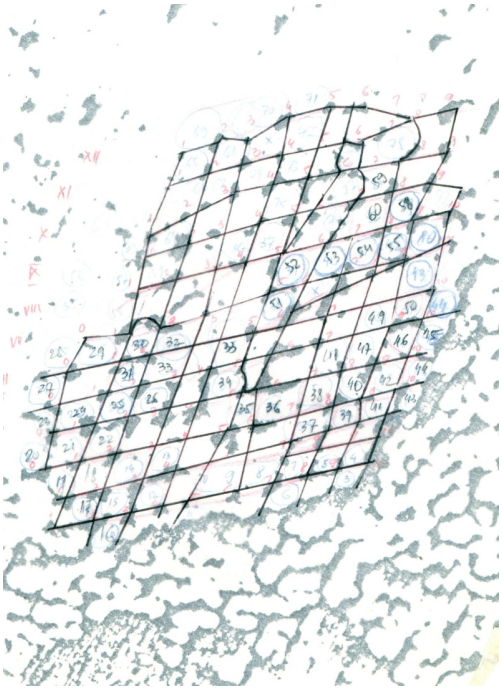

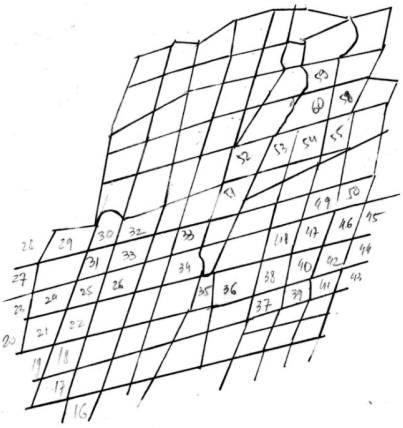

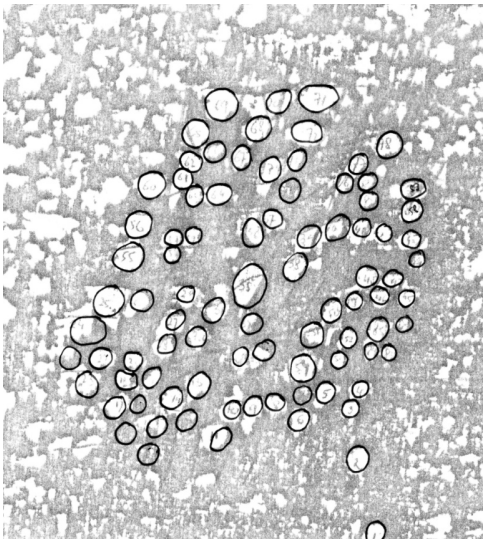

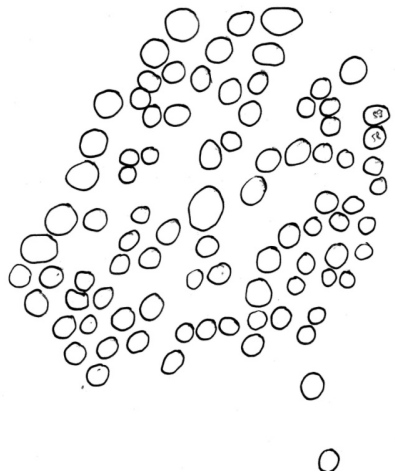

Fig. 49.

Fig. 49 shows tracings of particulate and pitted faces of GJ in Figs. 44-48 as steps in the attempt to find the best match of individual particles in the grid of pits. This diagram is similar to the one shown in Figs. 35 and 43.

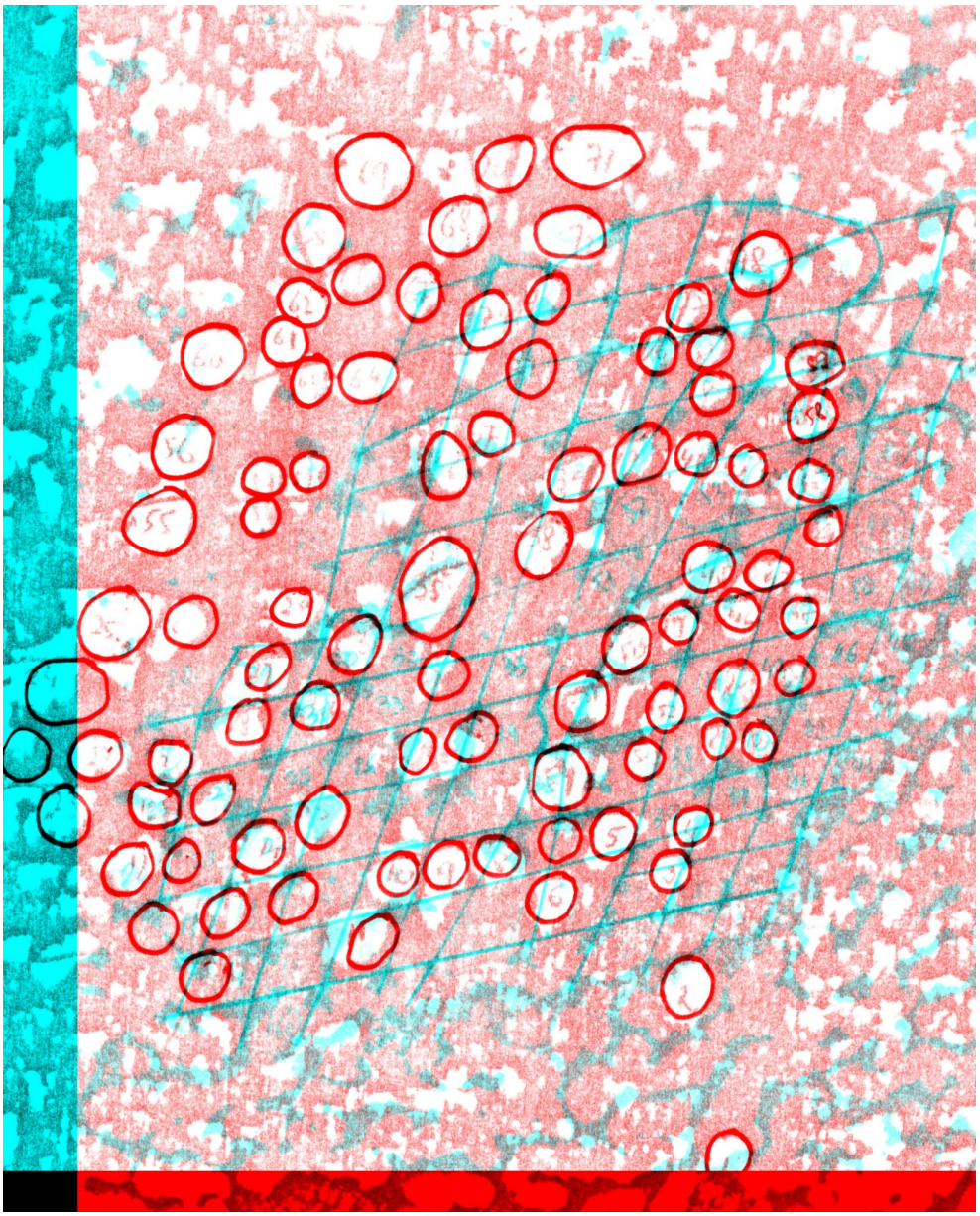

Fig. 50.

A computer-generated composite image is shown in Fig. 50. The way this color-coded image was created is explained in the description of pictures of "vegetable" models of GJ in the next chapter. Fig. 49 corresponds to Figures 59 and 66. In Fig. 50 the two left pictures of Fig. 49 have been superimposed. Thus, this composite image contains all four images from Fig. 49 combined together to show the best possible match of particles and pits. However, the ideal match has not been achieved here, because the topography of the E-face pitted grid is not ideally congruent with that of the particulate one in this GJ. It may result from a possible distortion of either the sample or the image. This might have occurred at the time of fracturing/replicating or taking the photograph in the EM. Furthermore, some particles are apparently missing from the regular grid on the P-face, which was also noted by DeMaziere (1986) as one of possible reasons for mismatching numbers of particles and pits. However, many of such missing particles can be still matched with their complementary spaces *between* pits on the E-face. Due to distortion of the membranes or their images, finding the right spots for individual particles (or their small groups) requires minor adjustments of the alignment by shifting the superimposed images. This cannot be done with the printed superimposed images in which the superimposed components are fixed in one final position. Despite this difficulty the composite picture in Fig. 50 shows well that the grid of pits resembles the general array of particles in the entire area of this small GJ, as if they were imprinted in each other. The pits (marked blue) fall hardly ever anywhere else *but* in the spaces between the particles (outlined red). The rhomboid grid of the pits fits the pattern of the inter-particle spaces fairly well. However, the images in Figs. 49 and 50 are flat (two-dimensional) projections of the replicas, while in reality the replicas are dramatically spatial (three-dimensional) objects. Therefore, only 3D imaging (as in Figs.20, 23, 31, 47, and 48) can adequately represent the spatial organization of the structural details contained in the replicas.

Tracing experiments on large-scale models

A picture of a pile of red peppers (Fig. 51) nicely stacked on a stand at the market can be used to illustrate how the regular grid of repeated morphological characteristics can be interpreted correctly, close to reality. This model from everyday life may also help to demonstrate how misinterpretations can be avoided. The complex relations between structural details observed in GJs may be better explained on such large-scale color models consisting of familiar elements.

Fig. 51. A stereo image of a regular array of red peppers similar to P-face particles.

The picture above (Fig. 51) is composed of two images mounted as a stereo pair. Although both pictures in the pair look very much alike, they differ slightly by the viewing angle and should be seen with the aid of a stereo viewer (Fig. 5). With some experience in handling the "Magic Eye"-type images, X-3D naked eye viewing method can be also successfully applied to obtain the 3D effect.

Similarly to tilting the sample on the EM goniometer stage, to create 3D images of large-scale objects, two consecutive photos were taken from a slightly different perspective. Instead of tilting the sample relative to the fixed column of the electron microscope, with the large-scale models the camera was being shifted and slightly tilted between the consecutive exposures. For 3D viewing, the prints of such photos are put side by side in reverse order (left image to right, right image to left). This image (Fig. 51), as well as other 3D images of vegetables in this chapter (Figs. 52, 53, 53, 58 and 59), was aligned for 3D viewing with the computer program "StereoPhoto Maker" downloaded from the Internet (http://stereo.jpn.org/eng/stphmkr/).

Three-dimensional viewing of this pile of vegetables clearly shows the benefits of stereo perception. The benefits of 3D imaging in light microscopy were reviewed in my previous article (Kordylewski 1996), while the advantage of 3D imaging for better recognition of particles in EM replicas was emphasized in my other papers (Kordylewski et al.

1983, 1965a, b, c, 1986).

The semi-regular hexagonal array of peppers (which resembles the pattern of P-face particles in GJ replicas) is the most distinct feature shown in Fig. 51. Furthermore, features of each pepper can be seen in great detail when viewed in 3D. In particular, green stems (at the locations analogous to those of GJ channels in the connexon) are sticking out of the plane of the picture in a spectacular and impressive way. In this stereo image, the depth of the spaces between individual peppers becomes particularly apparent with 3D inspection.

Although always black and white, the 3D electron micrographs of freeze-fractured replicas can appear equally spectacular when viewed in 3D (Figs. 19, 21, 28, 29, 30, 42, 45 and 46). Furthermore, binocular stereo vision of three-dimensional fine structure of replicated GJs greatly enhances the recognition of detail and helps to understand the spatial organization of the studied sample. Mere observation of traditional flat projections of the samples in the EM micrographs results in missing information, especially that regarding the shapes of objects and their spatial relations in samples like FF replicas.

The image in Fig. 51, as well as other 3D images in this chapter (Figs. 52, 53 and 59), were created with the 3D image processing software "StereoPhoto Maker" downloaded from the Internet (http://stereo.jpn.org/eng/stphmkr/). Such stereo images can be viewed with a stereo viewer (Fig. 5), or (after some practice) they can be directly seen in 3D by crossing the unaided (naked) eyes with the "magic eye"-style technique called X-3D. This method does not require any special 3D glasses or 3D screen. The observer has to keep crossing eyes until the left and right images overlap and fuse in the center into one well-focused image (reference to X-3D – magic eye).

Reprocessed with the anaglyph application of the same program, the stereo images can be coded with magenta and red colors (see Fig. 59) to be viewed with bicolor 3D spectacles, red filter over the right eye and blue filter over the left one.

The same 3D picture can be presented as an animated image to show the depth of the structure through simulation of rotational movement. The software quickly alternates between the two images taken at different angles (Fig. 51). Although at each time both eyes of the observer see a single flat image, thanks to the stroboscopic effect due to fast alternate inspection, a 3D perception of the image is achieved (see Fig. 53).

Another image of the piled artichokes (Fig. 52-61) was used in a similar way. These vegetables stacked up in a pile also display a distinct hexagonal pattern (Fig. 52). When positioned tightly together, roundish objects would spontaneously array themselves in such order. At the micro level, this is probably true also for the P-face particles in the gap junctional membrane of higher vertebrates.

However, the circular array of particles in the frog GJs (Figs. 12, 13, 14, 41, 42, and 43) cannot be explained in the same way. Thus the forces occurring between frog GJ particles somehow involved in holding them together in a circle still remain to be explained. Nevertheless, the spaces around the GJ particles deserve more attention. According to my observations, contrary to common views, GJ pits are located just there, between the particles.

Because of these striking structural analogies, in this "vegetable" model the artichokes can be regarded as suitable model of particles, while darkly shadowed spaces between them will be used to trace the analogs of pits.

Fig. 52

The same stereo image as in Fig. 52 is presented as an anaglyph image for 3D viewing with bi-color spectacles (Fig. 53).

Fig. 53. Example of an anaglyph to be viewed with bi-color spectacles for 3D effect.

The same stereo pair as in Figs. 52 and 53 is presented below as an animated image to show the depth of the structures by rotational movements (Fig. 54).

Fig. 54. Spatial details of the pile of artichokes are shown through alternate viewing of each image to simulate rotational motion of the images.

Although stereoimaging is very helpful in finding the right relations of the structural details, for the sake of simplicity, in this chapter single images (Fig. 55, 62) were used to produce tracings of complements (Figs. 56, 57, 63, 64) which were superimposed on each other (Figs. 60, 61, 66, 67, 68, 69, 70). As explained elsewhere in this article (see Fig. 7), I used a very similar method to superimpose the EM images of GJ faces, both as single images of P- and E- faces (Figs. 33 and 43) and their stereo views (Figs. 20, 23, 31, 32, 47 and 48).

Comparison of the stereo image and a single flat projection of the same scene illustrates an important issue. The appearance of a common object, like a vegetable, is familiar from real life, therefore the recognition of the structural details in the single flat image is relatively easy. Also the spatial relationship of these details can be

easily understood by referring to the experience with the well-known real large scale object. However, drawing any conclusion from the flat image of an unknown micro-object (e.g. the replica of cellular ultrastructure) may easily lead to misinterpretations of the spatial organization of the sample. This is because the information about the depths in the sample is lost in the commonly used two-dimensional projections of the image.

Fig. 55. Regular single photograph of the same scene as in Figs. 51, 52, and 53; the disadvantages of the flat projection of the spatial structures are evident when this flat image is compared to 3D views in Figs. 51, 52 and 53.

The above image (Fig. 55) was processed with a simple image processing software (www.nero.com) to yield images in Figs. 56 and 57. Converting the image to black and white, reversing and enhancing contrast resulted in obtaining a tracing shown below (Fig. 56) in which black contours represent artichokes (particles) from the picture above (Fig. 55). The spaces between them remain white in Fig. 54. The hexagonal array of the "particles" is distinct, while the spaces between them form a nice semi-regular hexagonal grid.

Formatted: Check spelling and grammar

Field Code Changed

Formatted: Check spelling and grammar

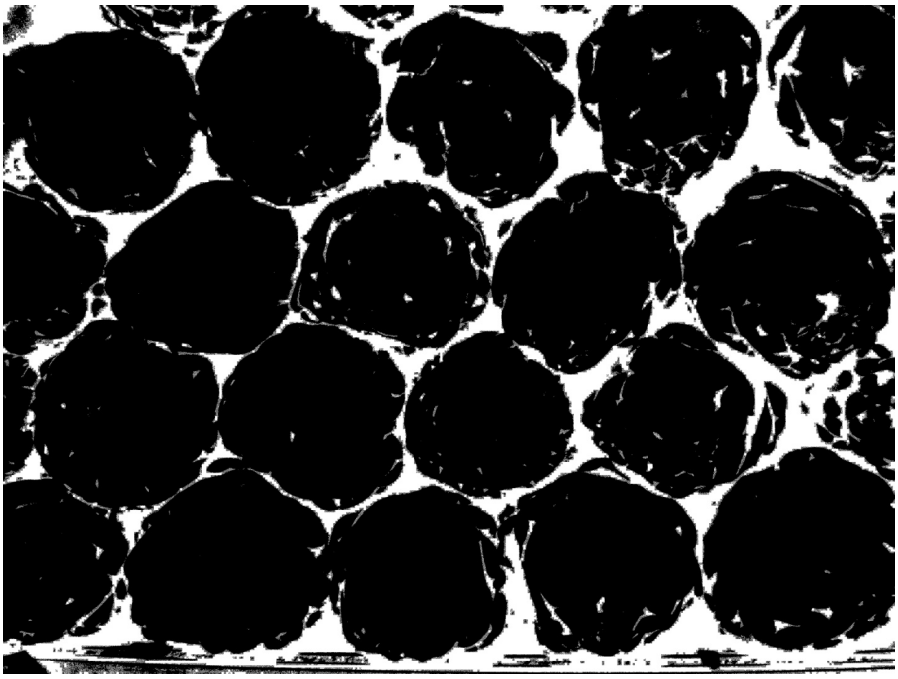

Fig. 56. Black silhouettes of artichoke “particles” of Fig. 54.

The image above (Fig. 56) has been reversed to obtain the image below (Fig. 57) in which the bodies of the artichokes (analogs of GJ particles) are white and the grid of spaces between them is black. In particular, the spaces between each three “particles” appear as distinct semi-triangular “nodes”. This again resembles the appearance of E-face pits in the electron micrographs of replicas of GJs (Figs. 20, 23, 31, 47, 48).

Fig. 57. Black grid of spaces between artichoke “particles” from Fig. 53; Triangular, or “bow-tie” shapes of spaces between “particles” are distinct and resemble the shadowed shapes of E-face pits. Comparison of the pattern in Fig. 56 with that in Fig. 57 helps to understand the relations between the hexagonal array of P-face particles and the rhomboid grid of complementary E-face pits in Figs. 49 and 50.

When a stereo pair of such tracing is used (Fig. 58), it becomes readily visible that these “nodes” represent “depressions” located between the white shapes of the “particles”.

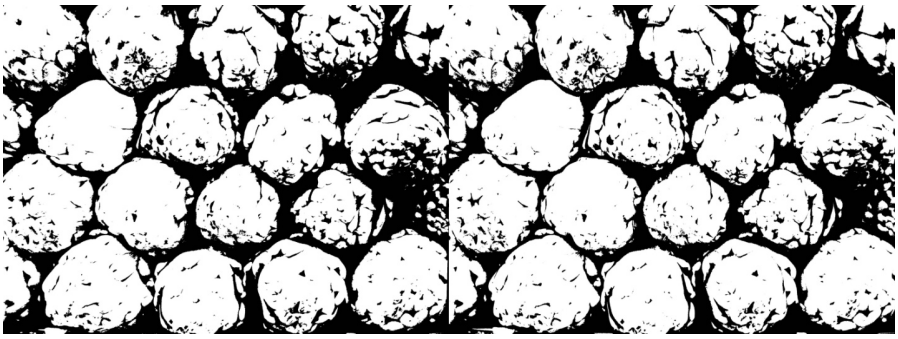

Fig. 58. Stereo view of the grid of spaces emphasizing convex outlines of "particles", and concave "pits" similar to those seen in GJ E-face.

The same 3D effect is obtained when the anaglyph image (Fig. 57) is viewed with the aid of bicolor 3D spectacles (red for the right eye, blue for the left eye).

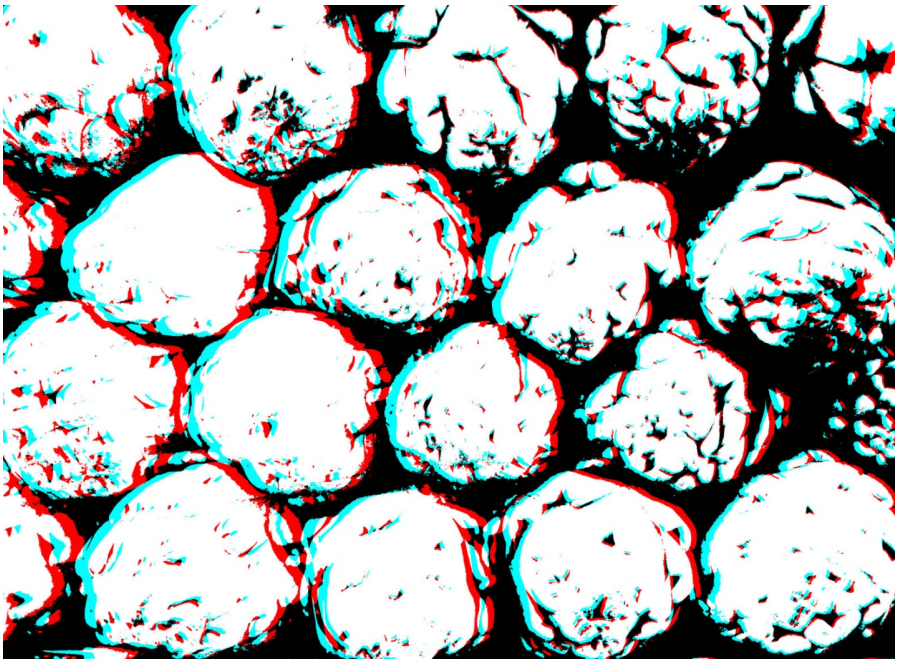

Fig. 59. Anaglyph of the image in Fig. 58.

The image below (Fig. 60) is a composite of two single images produced with another simple computer program "StereoPhoto Maker". Instead of the application normally used to align the images to be mounted as stereo-pairs (like the vegetable pictures in Figs. A and B) another application of this program was used, which is designed to combine two pictures to create an anaglyph stereo image, like the one in Fig. 59. In this application a blue tracing of one image was manually moved over the red tracing of the other image to align them appropriately. However, this is not a 3D image. The image in Fig. 56 was converted to make the "particles" red (with black outlines), while the image of the spaces in Fig. 57 was turned into blue grid. By playing with red artichoke "particles" of Fig. 54 I attempted to find the best fit for them in the blue grid. Even if I missed the original (correct) match by one or more rows, the best fit was always when the nodes of the grid were falling into the spaces between the particles, as shown in Fig. 58.

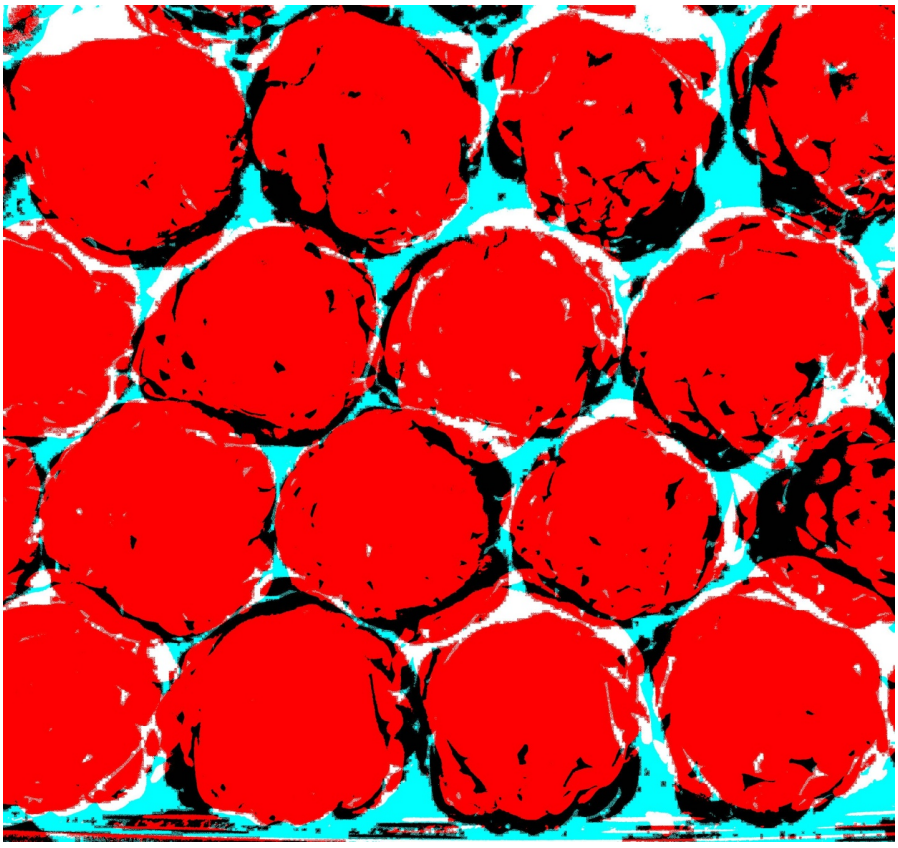

Fig. 60. Near-perfect match of tracings of the artichoke "particles"

(red/black) with “pits” (white/magenta). This is not a stereo view.

It was also possible to “force” the grid in such a manner that the “nodes” would be aligned with the centers of the particles (Fig. 61). However, similarly as in the EM images of the replicated GJs, such fit appears obviously incorrect. Only 3 out of 6 “nodes” in each unit of the grid can be positioned on top of the particles, while the other three still fall on the semi-triangular spaces between the red “particles”. Such match is not right, the grid is evidently off register (Fig. 61).

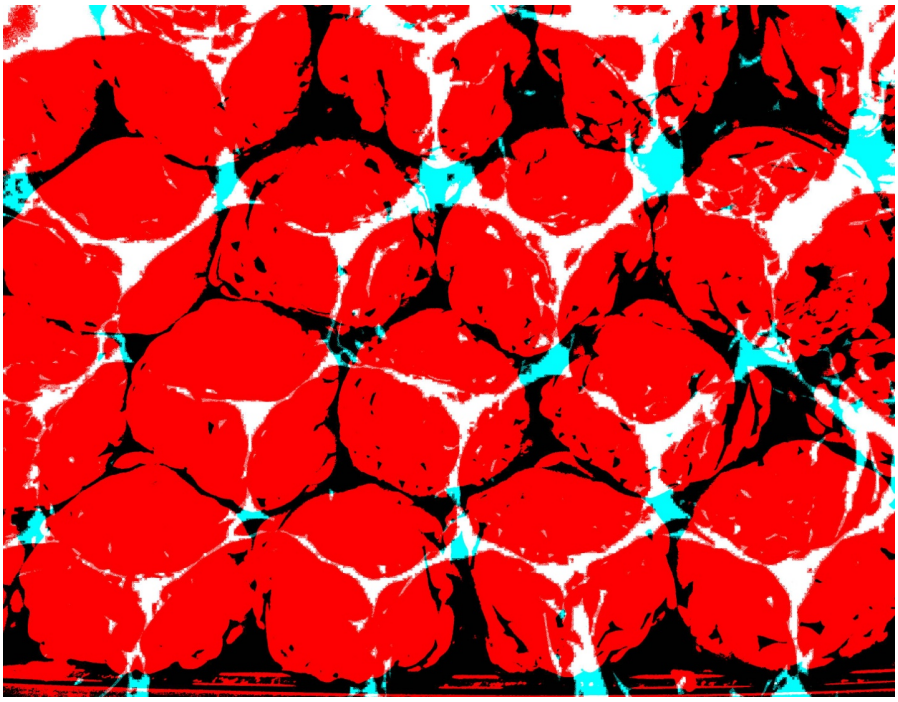

Fig. 61. Mismatch of “particles” (red/black) and “pits” (white/magenta) when “pits” are forced to be positioned on tops of the “particles”. Such a model of GJ particles and pits has been used up to the present and needs to be corrected.

A similar tracing experiment was performed with the image of green peppers (Fig. 62)

Fig. 62. Stacked peppers form a hexagonal array. In this model the vegetables may be compared to the particles with the "GJ channels" represented by the broken off stems.

In Fig. 63 the peppers were converted into black particles by image processing, while the grid of the spaces between them remained white.

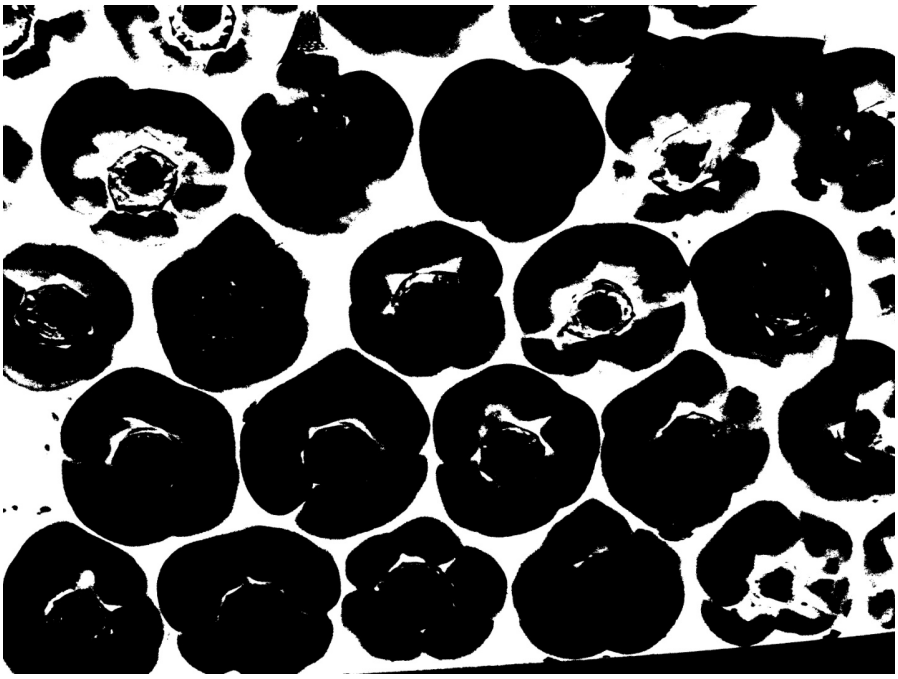

Fig. 63. Black silhouettes of the pepper “particles” of Fig. 62 (similar to Fig. 52).

In Fig. 64 the grid of white spaces of Fig. 63 was reversed to black. The grid consists of units of six semi-triangular “nodes” which form a hexagonal network of “rings”. The network of such rings can be fitted with the hexagonal pattern of the particles of Fig. 63. At the same time, imaginary horizontal and angled lines following this grid would create a rhomboid network similar to that of the pits seen in Figs. 35 a, b and 50.

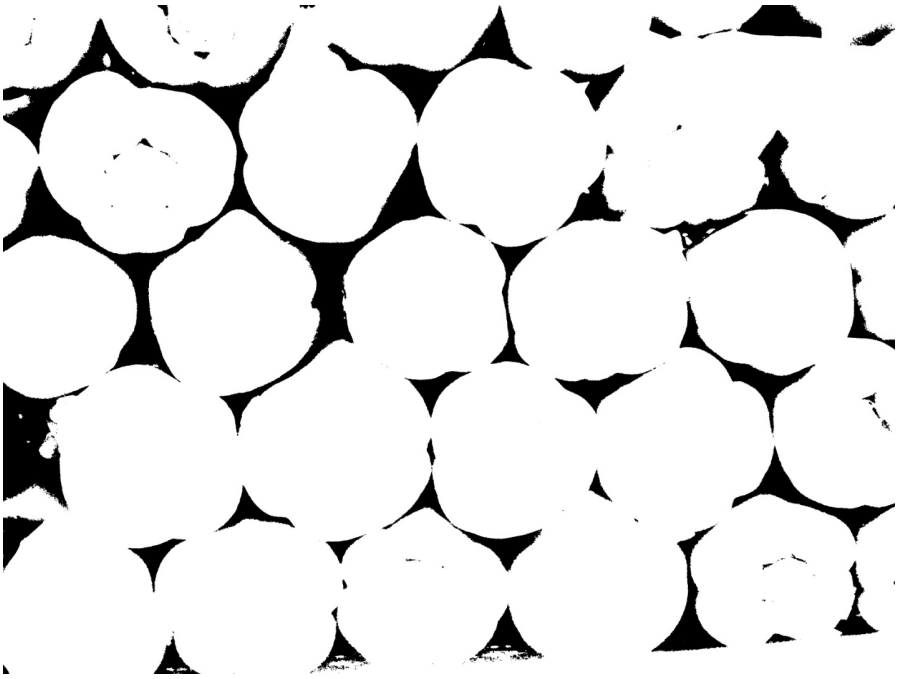

Fig. 65. Black tracings of spaces between peppers (“particles”), similar to Fig. 57.

In Fig. 66 the shapes of the bodies of the peppers (particles) were colored blue in an attempt to fit them with the black grid of pits. Fig.66 shows incorrect alignment of the “nodes” (pits) with the centers of the “particles”. The sections of the grid that fall over the particles remain black, while other parts of the grid that fall in the white spaces between the “particles” are highlighted red. This match (Fig. 66) appears unnatural because it is evidently out of register. Nevertheless, such a misleading model, with pits aligned with the tops of particles, has been uncritically accepted and used over decades to illustrate GJ structure incorrectly.

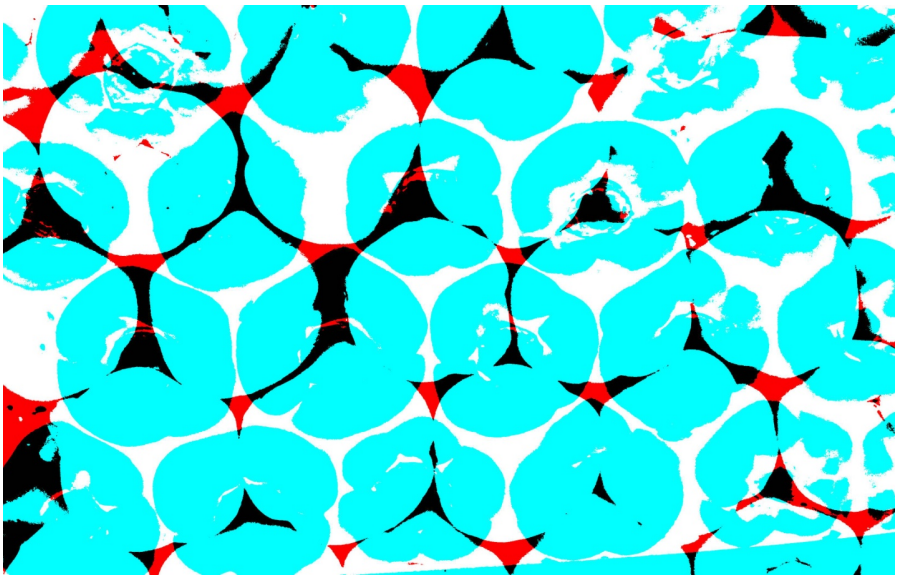

Fig. 66. Particles (magenta) and pits (black) of Figs. 64 and 65, respectively, are combined to illustrate the incorrect concept of alignment of particles and pits, still commonly applied to explain GJ structure.

Fig. 67 shows the ideal match which is correct as we know it from real life: "nodes" (pits) are perfectly aligned with the spaces between particles (peppers). Artichokes (particles) are blue, and the spaces between them (where the pits would be found in GJ) are filled with red color. This fitting, so obvious in the case of peppers, has not been considered for GJ particles and pits before. My experiments with 3D images of complementary replicas of the same GJ split into complementary half-leaves and displayed together undoubtedly indicated the correct match: the pits located outside particles in the spaces between them, as illustrated in the large-scale model in Figs. 67 and 68.

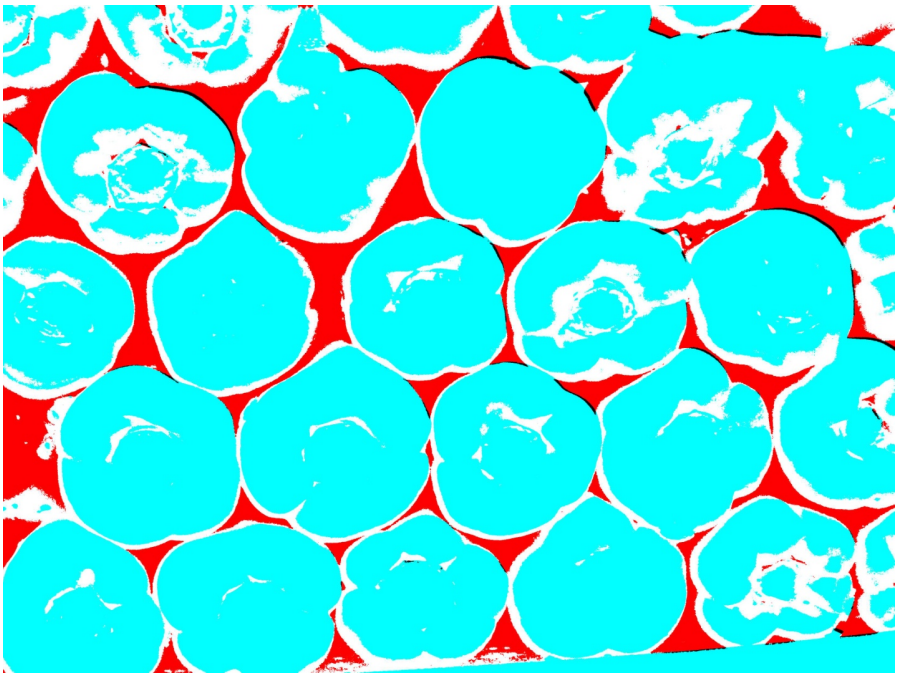

Fig. 67. Correct matching of “particles” and “pits” in the pepper model which shows appropriate alignment of pits (red) with particles (magenta).

The two subsequent figures show that a similar correct match (Fig. 69) or mismatch (Fig. 69) can be obtained when the original images of the (vegetable) large-scale models of the GJ structure are used.

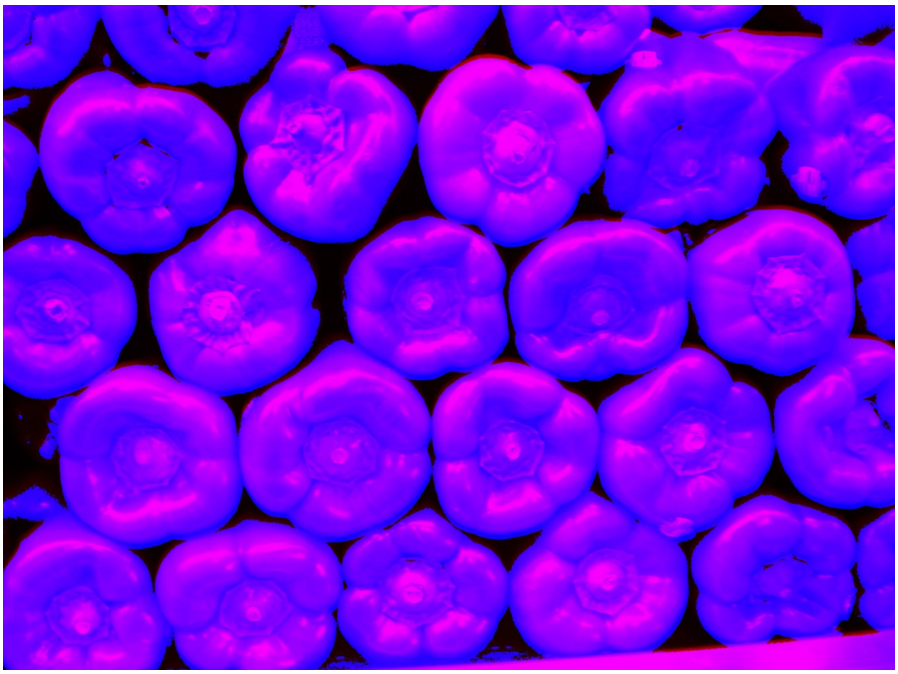

Fig. 68

Fig. 68 resembles very much the central panels in the original triplefold mounts of stereo images of electron micrographs in Figs.20, 23, 31, 47 and 48. In both the vegetable model and GJ, pits do not match the particles, but they fall in the spaces between particles.

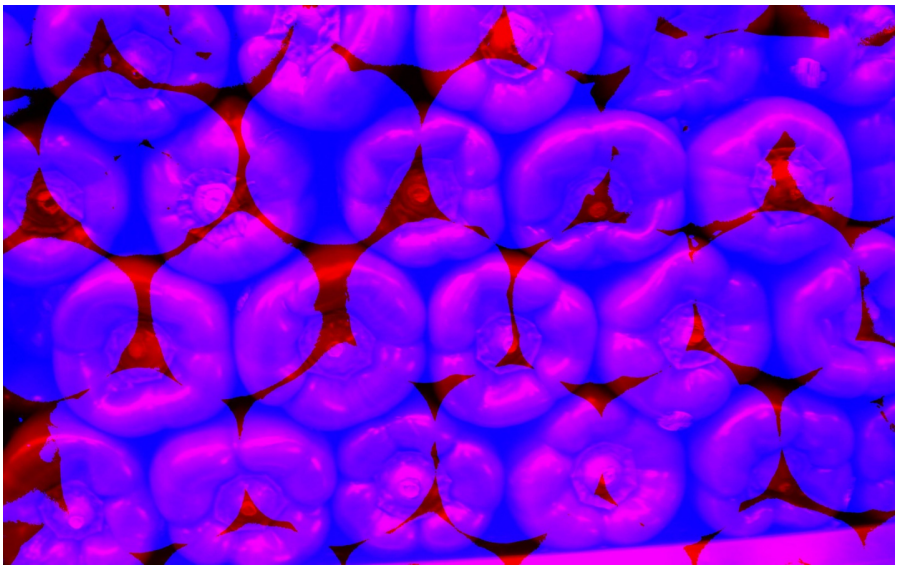

Fig. 69

Fig. 69 shows the mismatch of the tracing of the spaces superimposed out of place on the image of hexagonally arrayed peppers. The misalignment is obvious, although it can be forced, if one would anticipate the right position of dark triangular profiles on top of the broken off stems. Such misalignment has been continuously presented as the right one in the currently used speculative models of GJ organization. These models have never before been verified by actually putting back together E-face pits and P-face particles in composite 3D images. Such images published for the first time in this work are shown in Figs. 20, 23, 31, 47 and 48. They show that matching pits with the spaces between particles is the only correct way. Forcing the images of GJ pits on top of the GJ particles gives similar mismatched image, like the one of the model peppers above in Fig. 69.

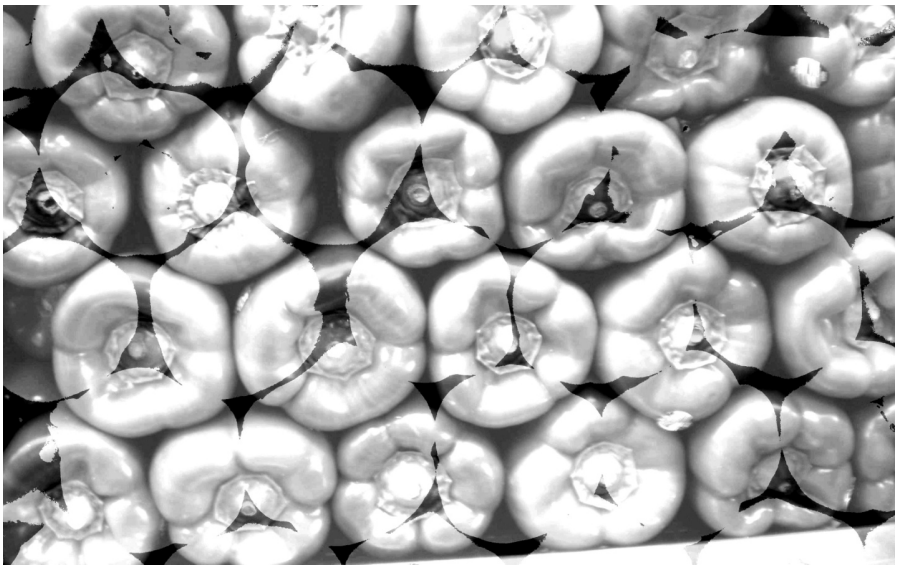

Fig. 70

Conclusion

This article describes my experiments with the images of GJ faces (E and P) in the electron micrographs in the attempts to fit them correctly, to demonstrate that the currently accepted model of GJ structure is not correct. Since electron micrographs are always black and white, a black and white version of the tracings of the vegetable model is shown in Fig. 70. Despite lack of color it shows once again that the dark "pits" can be incorrectly aligned with the centers of the "particles" (peppers), while their right locations remain in the spaces between "particles" (peppers).

The investigators who previously coined and popularized the "pits on particles" model of the freeze-fractured GJs (e.g., Goodenough and Revel, 1970, Chalcroft and Bullivant, 1970, Caspar et al., 1977, Baker, et al., 1983, De Maziere, et al. 1987)

) did not have high power stereo images available, neither did they use complementary replicas to put back together the images of split GJs. In their studies they merely compared analogous areas of different GJs. Only DeMaziere (1986) used complementary replicas (like the ones in my studies), but she did not observe them in 3D. I found that the superimposition of the high power 3D images of complementary areas of E-face and P-face of the GJ, which were forming a "single object"

before splitting GJ membranes into two faces is essential to finding a correct match. Without such inspection a purely hypothetical idea of pits being "scars" after removed particles may seem plausible, but is wrong. In view of my current findings such "scar" model is not adequate to the GJ real structure. I was able to dispute this model only by having preserved complementary fragments of the same GJ, producing complementary replicas of these fragments, examining their structure on 3D high power electron micrographs to find matches exactly in the areas which adhered to each other being split. In addition, traditional photographic and tracing methods, the onset of new modern digital technologies allowed me to review the traditional photographic images and helped to confirm this substantial revision of the GJ model used so far. I strongly believe that my new model of GJ structure, explained in detail in this work and shown in Figs. 15 and 16, is the only accurate interpretation of the relations of pits and particles, adequate to the organization of the unsplit GJ in the native cell membranes.

Acknowledgments

The author is indebted to the late Dr. Ernest Page for making available the facilities of his laboratory for performing this study. The advice shared by Dr. Theodore Karrison on the quantitative analysis of complementary P- and E-faces is greatly appreciated. I also thank Dr. January Weiner and Ms. Kathy Hirsh for the artist's renditions of gap junctional structure.

This work has been supported by National Heart, Lung, and Blood Institute Grants HL 10503 and HL 20592.

An abstract related to this work has been previously published (Kordylewski and Page, 1985).

References

Baker TS, Caspar DLD, Hollingshead CJ, Goodenough DA (1983) Gap junction structures. IV. Asymmetric features revealed by low irradiation microscopy. J. Cell Biol. 96: 204-216

Bullivant S (1974) Freeze-etching techniques applied to biological membranes. Phil. Trans. R. Soc. Lond. B 268: 5-14

Caspar DLD, Goodenough DA, Makowski L, Phillips WC (1977) Gap junction structures. I. Correlated electron microscopy and X-ray diffraction. J. Cell Biol. 74: 605-628

Chalcroft JP, Bullivant S (1970) An interpretation of liver cell membrane and junction structure based on observation of freeze-fracture replicas of both sides of the fracture. J. Cell Biol. 47: 49-60

De Maziere AMGL, Scheuermann DW, Aergtgeerts PAPM (1987) Complementarity of particles and pits in freeze-fractured hepatic and cardiac gap junctions. Jour. Membrane Biol. 97, 107-115

Goodenough DA, Revel JP (1970) A fine structural analysis of intercellular junctions in the mouse liver. J. Cell Biol. 45: 272-290

Kordylewski L, Karrison T, Page E (1983) P-face particle density of freeze-fractured vertebrate cardiac plasma membrane. Am. J. Physiol. 245: H992-H997

Kordylewski L, Page E (1985a) Are gap junctional pits and particles complementary structures? Biophysical Journal, 47, 2, 2, 506a

Kordylewski L, Goings G, Karrison T, Page E (1985b) Developmental changes in internal structure of chick heart plasma membrane. Devel. Biol. 112 (2), 485-488

Kordylewski L, Karrison T, Page E (1985c) Measurements on the internal structure of freeze-fractured cardiac plasma membrane. Am. J. Physiol. 248: H297-H30

Kordylewski L, Karrison T, Page E (1986) Developmental changes in P-face and E-face particle densities of Xenopus cardiac muscle plasma membrane. Tissue and Cell, 18 (5), 793-801

Kordylewski L, Goings GE, Page E (1993) Rat atrial myocyte plasmalemmal caveolae in situ. Reversible experimental increases in caveolar size and in surface density of caveolar necks. Circulation Research, 73 (1), 135-146

Kordylewski L, Saner D, Lal R (1994) Atomic force microscopy of freeze-fracture replicas of rat atrial tissue. J. Micr. 173 (3), 173-81

Kordylewski L (1996) 3-D Microscopy. Postepy Biologii Komorki 23, 635-656

Saferstein R ed. (2002) The Forensic Science Handbook, Volume I, 2nd Edition. New Jersey: Pearson Education, Inc., Chapter 4: Forensic Glass Comparisons

Wrigley NG, Brown E, Chillingworth RK (1984) Reversible structure transition in gap junction under Ca^{++} control seen by high-resolution electron microscopy. Biophys. J. 45: 201-207

Acronyms and some terms used

3-D	**three dimensional**
AFM	**Atomic Force Microscope, electronic instrument to image molecular organization of samples**
C	**carbon**
C_1	**cell #1**
c_1	**cytoplasm of cell #1**
C_2	**cell #2**
c_2	**cytoplasm of cell #2**
cardiac	**related to heart as an organ or tissue**
caveola	**single pocket in the cell membrane engaged in endocytosis**
caveolae	**multiple pockets or depressions in the cell membrane**
caveolar	**pertaining to caveolae**
cell	**basic unit of living organism (their tissues and organs), wrapped in cell membrane**
cellular	**pertaining to cell/cells**
Comparative Microscopy	**studying microstructure of the same sample with various types of microscopy by comparing its different images**
congruent	**fitting well, having same shape, although not identical**
connexin	**protein of which connexons are built**
connexon	**building brick of GJ seen with EM as a particle**

cytoplasm	**cell body within cell membrane**
EF	**E-face**
electron micrographs	**photographic images obtained with electron microscope**
electron microscope	**complex electronic instrument to see ultrastructure of a sample**
EM	**Electron Microscopy**
endocytosis	**intake of extracellular matter by cells**
extra-cellular	**outside cell**
extra-junctional	**outside junction**
FF	**freeze fracture**
freeze fracturing	**preparatory technique aiming at obtaining replicas of samples frozen with LN2**
gap	**extracellular space narrowed in the GJ area**
GJ	**gap junction, specialized area of cell membranes of joined cells**
IMP	**intramembrane particle**
intercellular	**within cell**
intracellular	**between cells**
junctional	**pertaining to junction**
L_1	**layer originally belonging to membrane of cell #1**
L_2	**layer originally belonging to membrane of cell #2**
light microscopy	**seeing detail of the sample in visible light with microscope**
lipid bilayer	**basic structural component of cell membrane consisting of two layers of lipids**
lipid	**basic chemical component of cell membrane layers**

LN_2	**liquid nitrogen used to freeze tissue samples**
m_1	**membrane of cell #1,**
m_2	**membrane of cell #2**
Magic Eye	**method of seeing 3D graphic images by crossing eyes**
micrographs	**photographic images obtained with microscope**
microscope	**complex optical instrument to see detail unavailable to unaided eye**
microscopy	**knowledge of microscopic objects**
muscle tissue	**tissue specialized in contractions**
myocytes	**muscle tissue cells**
organ	**functional unit of each living body, composed of tissues, e.g. heart composed of cardiac cells (myocytes, Purkinje cells)**
organelle	**structural detail of cell with distinct function**
P_1	**particles of the membrane of cell #1**
P_2	**particles of the membrane of cell #2**
Parallel	**similar, matching, oriented in the same direction**
PF	**P-face**
pit	**darkly shadowed depression in the junctional membrane seen on the E-face and believed to be marking the center of the removed particle which is removed (in single replicas) or travels with P-face to the other complementary replica (in double replicas); in this article pits are revealed to be shadowed depressions of the E-face layer covering the complementary set of P-face particles hidden under it – pits are proven to lie in the spaces between particles (see diagrams in Figs. 15-17).**
protein	**basic chemical component of cell membrane particles**

Pt	**platinum**
Purkinje strands	**conductive tissue of heart composed of specialized cardiac myocytes which transfer electric signals; GJs play crucial role in their functions**
replica	**Pt/C casting of the freeze-fractured sample**
replica A	**specimen observed and photographed with EM**
replica B	**replica complementary to replica A obtained from the same tissue sample split into two portions with FF**
SEM	**Scanning Electron Microscope, electronic instrument to see high resolution images of sample surface**
stereo	**related to three dimensional perception**
stereo pair	**two pictures differing by viewing angle to merge into 3D image**
stereo viewer	**simple two lens device to see 3D effect in stereo pairs of images (Fig. 4)**
stroboscopic effect	**merging visually two consecutive images to see differences**
TEM	**Transmission Electron Microscope (Fig. 4)**
tissue	**component of each living body, composed of cells**
topography	**shape referring to hilly landscape or terrain**
ultrastructure	**fine structure of cell details beyond resolution of light microscope**
X	**image magnification factor (magnified x times)**
X-3D	**“Magic Eye”-style method of 3D perception of images by looking at the stereo pair of pictures without using stereo viewer, only with eyes crossed**